

# Galaxy Cluster Masses Without Non-Baryonic Dark Matter

J. R. Brownstein\* and J. W. Moffat†

*The Perimeter Institute for Theoretical Physics, Waterloo, Ontario, N2J 2W9, Canada, and  
Department of Physics, University of Waterloo, Waterloo, Ontario N2Y 2L5, Canada*

Submitted 2005 July 8.

## ABSTRACT

We apply the modified acceleration law obtained from Einstein gravity coupled to a massive skew symmetric field,  $F_{\mu\nu\lambda}$ , to the problem of explaining X-ray galaxy cluster masses without exotic dark matter. Utilizing X-ray observations to fit the gas mass profile and temperature profile of the hot intracluster medium (ICM) with King “ $\beta$ -models”, we show that the dynamical masses of the galaxy clusters resulting from our modified acceleration law fit the cluster gas masses for our sample of 106 clusters without the need of introducing a non-baryonic dark matter component. We are further able to show for our sample of 106 clusters that the distribution of gas in the ICM as a function of radial distance is well fit by the dynamical mass distribution arising from our modified acceleration law without any additional dark matter component. In previous work, we applied this theory to galaxy rotation curves and demonstrated good fits to our sample of 101 LSB, HSB and dwarf galaxies including 58 galaxies that were fit photometrically with the single parameter  $(M/L)_{stars}$ . The results there were qualitatively similar to those obtained using Milgrom’s phenomenological MOND model, although the determined galaxy masses were quantitatively different and MOND does not show a return to Keplerian behavior at extragalactic distances. The results here are compared to those obtained using Milgrom’s phenomenological MOND model which does not fit the X-ray galaxy cluster masses unless an auxiliary dark matter component is included.

**Key words:** dark matter — galaxies: clusters: general — galaxies: kinematics and dynamics — gravitation — X-rays: galaxies: clusters

## 1 INTRODUCTION

The question of galaxy rotation curves and cluster masses has been known to require some form of energy density that makes its presence felt only by its gravitational effects since Zwicky (1933) analyzed the velocity dispersion for the Coma cluster. By 1959 there were eight galaxy rotation curves available from radio observations demonstrating a “flat rotation velocity”. In Brownstein & Moffat (2005) – our study of galaxy rotation curves without non-baryonic dark matter – we demonstrated good fits to our sample of 101 LSB, HSB and dwarf galaxies including 58 galaxies that were fit photometrically with the single parameter  $(M/L)_{stars}$  (29  $B$ -band and 29  $K$ -band). As a follow-up, we apply here the same framework to the question of X-ray galaxy cluster masses (Moffat 2005a,b; Brownstein & Moffat 2005).

In this framework, we apply a generalization of

Einstein’s general relativity (GR) based on a pseudo-Riemannian metric tensor and a skew symmetric rank three tensor field  $F_{\mu\nu\lambda}$ , called metric-skew-tensor-gravity (MSTG). A renormalization group (RG) framework (Reuter & Weyer 2004a,b) for MSTG was developed to describe the running of the effective gravitational coupling constant  $G$ , and the effective coupling constant  $\gamma_c$  that measures the strength of the coupling of the  $F_{\mu\nu\lambda}$  field to matter. A momentum cutoff identification  $k = k(x)$  associates the RG scales to points in spacetime. For the static, spherically symmetric solution, the RG flow equations allow a running with momentum  $k$  and proper length  $\ell(r) = 1/k$  for the effective Newtonian coupling constant  $G = G(r)$ , the coupling constant  $\gamma_c = \gamma_c(r)$ , and the effective mass of the skew field  $\mu = \mu(r)$  where  $r$  denotes the radial coordinate. The form of  $G(r)$  as a function of  $r$ , obtained from the modified Newtonian acceleration law, leads to agreement with solar system observations, terrestrial gravitational experiments and the binary pulsar PSR 1913+16 observations, while strong renormalization

\* [jbrownstein@perimeterinstitute.ca](mailto:jbrownstein@perimeterinstitute.ca)

† [john.moffat@utoronto.ca](mailto:john.moffat@utoronto.ca)

effects in the infrared regime at large distances lead to fits to galaxy rotation curves and X-ray cluster masses. In [Moffat \(2005b\)](#), a scalar-tensor-vector gravity theory is formulated, which yields the same weak field modified acceleration law as in MSTG [Moffat \(2005a\)](#), and equations that describe an effective running of  $G$ ,  $\gamma_c$  and  $\mu$  with space and time.

A fit to the bulk properties (the gas mass) of 106 X-ray galaxy clusters is achieved without exotic dark matter by a best fit result using a nonlinear least-squares fitting routine including estimated errors for the one free parameter in the RG flow equations,  $M_0$ , which fully describes the large distance renormalization of Newton's constant,  $G_\infty$ . The running of Newton's constant,  $G(r)$ , is fully constrained by choosing the remaining free parameter in the RG flow equations,  $r_0$ , to take on a value proportional to the scale of the galaxy cluster (for small clusters with galactic scale ICM gas masses) or to take on a particular constant value for the majority of the regular size galaxy clusters (where the ICM gas mass dominates over the masses of the individual galaxies). Thus, the individual cluster mass profiles as functions of radial position throughout the range of X-ray observations are parameter free predictions; and are consistent with X-ray observed gas mass profiles without exotic dark matter.

The galaxy cluster's bulk properties fit and the specific fit to the individual clusters are compared to those obtained using Milgrom's phenomenological MOND model which does not fit the X-ray galaxy cluster masses unless an auxiliary dark matter component is included ([Sanders 2003](#)). [The & White \(1988\)](#) were able to account for the MOND discrepancy between the X-ray observationally determined gas mass and the dynamical mass of the Coma cluster by increasing the MOND acceleration by a factor of four greater than that used to fit the galaxy rotation curves. [Aguirre et al. \(2001\)](#) present evidence from the central 200 kpc of three clusters implying that MOND is inconsistent with the observed temperature gradient which inflates the discrepancy in the MOND acceleration to a factor of  $\sim 10$ . More recently, [Pointecouteau & Silk \(2005\)](#) use X-ray data from the XMM-NEWTON satellite for eight clusters of varying temperature and masses to place constraints on the use of the MOND phenomenology. Without treating the MOND acceleration as a free parameter as opposed to a universal constant, MOND predicts dynamical masses greatly in excess of the X-ray observations – necessitating the ad hoc addition of dark matter to explain away the missing mass. We are able to show that there is no missing mass when applying the MSTG acceleration law to galaxy clusters.

## 2 ISOTROPIC ISOTHERMAL MODEL

Recent observations from the XMM-NEWTON satellite suggest that the intracluster medium (ICM) is very nearly isothermal inside the region defined by the X-ray emission with temperatures ranging from  $\approx 1$ –15 keV (or  $10^7$ – $2 \times 10^8$  K) for different clusters ([Arnaud et al. 2001b](#)). The combination of the observed density profile,  $n_e(r)$ , and the temperature profile,  $T(r)$ , obtained from X-ray observations of the galaxy cluster leads to a pressure profile,  $P(r)$ , which directly leads to a mass profile,  $M(r)$ , by assuming the gas

is in nearly hydrostatic equilibrium with the gravitational potential of the galaxy cluster. Within a few core radii, the distribution of gas within a galaxy cluster may be fit by a King “ $\beta$ -model”. The observed surface brightness of the X-ray cluster can be fit to a radial distribution profile ([Chandrasekhar 1960](#); [King 1966](#)):

$$I(r) = I_0 \left[ 1 + \left( \frac{r}{r_c} \right)^2 \right]^{-3\beta+1/2}, \quad (1)$$

resulting in best fit parameters,  $\beta$  and  $r_c$ . A deprojection of the  $\beta$ -model of equation (1) assuming a nearly isothermal gas sphere then results in a physical gas density distribution ([Cavaliere & Fusco-Femiano 1976](#)):

$$\rho(r) = \rho_0 \left[ 1 + \left( \frac{r}{r_c} \right)^2 \right]^{-3\beta/2}, \quad (2)$$

where  $\rho(r)$  is the ICM mass density profile. Provided the number density,  $n$ , traces the actual mass, we may assume that  $n(r) \propto \rho(r)$ , which according to [Reiprich \(2001\)](#) is explicitly

$$\rho_{\text{gas}} \approx 1.17 n_e m_p, \quad (3)$$

and rewrite equation (2)

$$n_e(r) = n_0 \left[ 1 + \left( \frac{r}{r_c} \right)^2 \right]^{-3\beta/2}. \quad (4)$$

For a spherical system in hydrostatic equilibrium, the structure equation can be derived from the collisionless Boltzmann equation

$$\frac{d}{dr}(\rho(r)\sigma_r^2) + \frac{2\rho(r)}{r}(\sigma_r^2 - \sigma_{\theta,\phi}^2) = -\rho(r)\frac{d\Phi(r)}{dr}, \quad (5)$$

where  $\Phi(r)$  is the gravitational potential for a point source,  $\sigma_r$  and  $\sigma_{\theta,\phi}$  are mass-weighted velocity dispersions in the radial ( $r$ ) and tangential ( $\theta, \phi$ ) directions, respectively. For an isotropic system,

$$\sigma_r = \sigma_{\theta,\phi}. \quad (6)$$

The pressure profile,  $P(r)$ , can be related to these quantities by

$$P(r) = \sigma_r^2 \rho(r). \quad (7)$$

Combining equations (5), (6) and (7), the result for the isotropic sphere is

$$\frac{dP(r)}{dr} = -\rho(r)\frac{d\Phi(r)}{dr}. \quad (8)$$

For a gas sphere with temperature profile,  $T(r)$ , the velocity dispersion becomes

$$\sigma_r^2 = \frac{kT(r)}{\mu m_p}, \quad (9)$$

where  $k$  is Boltzmann's constant,  $\mu \approx 0.609$  is the mean atomic weight and  $m_p$  is the proton mass. We may now substitute equations (7) and (9) into equation (8) to obtain

$$\frac{d}{dr} \left( \frac{kT(r)}{\mu m_p} \rho(r) \right) = -\rho(r)\frac{d\Phi(r)}{dr}. \quad (10)$$

Performing the differentiation on the left hand side of equation (8), we may solve for the gravitational acceleration:

$$a(r) \equiv -\frac{d\Phi(r)}{dr}$$

$$= \frac{kT(r)}{\mu m_p r} \left[ \frac{d \ln(\rho(r))}{d \ln(r)} + \frac{d \ln(T(r))}{d \ln(r)} \right]. \quad (11)$$

For the isothermal isotropic gas sphere, the temperature derivative on the right-hand side of equation (11) vanishes and the remaining derivative can be evaluated using the  $\beta$ -model of equation (2):

$$a(r) = -\frac{3\beta kT}{\mu m_p} \left( \frac{r}{r^2 + r_c^2} \right). \quad (12)$$

### 3 MASS PROFILES

Given an isotropic density distribution,  $\rho(r)$ , the associated mass profile is

$$M(r) = 4\pi \int_0^r \rho(r') r'^2 dr', \quad (13)$$

where  $M(r)$  is the total mass contained within a sphere of radius  $r$ . For the  $\beta$ -model of equation (2), we may approximate the integral of equation (13) for  $r \gg r_c$  and  $\beta < 1$  (Reiprich 2001):

$$M(r) \approx \frac{4\pi \rho_0 r_c^3}{3(1-\beta)} \left( \frac{r}{r_c} \right)^{3(1-\beta)} \leftarrow \{r \gg r_c \text{ and } \beta < 1\}. \quad (14)$$

This result clearly diverges in the limit as  $r \rightarrow \infty$ ; but galaxy clusters are observed to have finite spatial extent. This allows an approximate determination of the total mass of the galaxy cluster by first solving equation (2) for the position,  $r_{\text{out}}$ , at which the density,  $\rho(r_{\text{out}})$ , drops to  $\approx 10^{-28}$  g/cm<sup>3</sup>, or 250 times the mean cosmological density of baryons:

$$r_{\text{out}} = r_c \sqrt{\left( \frac{\rho_0}{10^{-28} \text{ g/cm}^3} \right)^{2/3\beta} - 1}. \quad (15)$$

Then, provided  $\beta < 1$ ,

$$M_{\text{gas}} \approx \frac{4\pi \rho_0 r_c^3}{3(1-\beta)} \left( \frac{r_{\text{out}}}{r_c} \right)^{3(1-\beta)}. \quad (16)$$

The dynamical mass in Newton's theory of gravitation can be obtained as a function of radial position by replacing the gravitational acceleration with Newton's Law:

$$a_N(r) = -\frac{G_0 M(r)}{r^2}, \quad (17)$$

where  $G_0$  is Newton's "bare" gravitational constant so that equation (11) can be rewritten as

$$M_N(r) = -\frac{r}{G_0 \mu m_p} \frac{kT}{r} \left[ \frac{d \ln(\rho(r))}{d \ln(r)} + \frac{d \ln(T(r))}{d \ln(r)} \right], \quad (18)$$

and the isothermal  $\beta$ -model result of equation (12) can be rewritten as

$$M_N(r) = \frac{3\beta kT}{\mu m_p G_0} \left( \frac{r^3}{r^2 + r_c^2} \right). \quad (19)$$

Similarly, the dynamical mass in MSTG can be obtained as a function of radial position by substituting the MSTG gravitational acceleration law (Moffat 2005a,b; Brownstein & Moffat 2005):

$$a(r) = -\frac{G(r)M}{r^2}, \quad (20)$$

so that our result for the isothermal  $\beta$ -model becomes

$$M_{\text{MSTG}}(r) = \frac{3\beta kT}{\mu m_p G(r)} \left( \frac{r^3}{r^2 + r_c^2} \right). \quad (21)$$

We can express this result as a scaled version of equation (18) or the isothermal case of equation (19):

$$\begin{aligned} M_{\text{MSTG}}(r) &= \frac{G_0}{G(r)} M_N(r) \\ &= \left\{ 1 + \sqrt{\frac{M_0}{M_{\text{MSTG}}(r)}} \left[ 1 - \exp(-r/r_0) \left( 1 + \frac{r}{r_0} \right) \right] \right\}^{-1} M_N(r), \end{aligned} \quad (22)$$

where we have made explicit the form of the running of  $G(r)$  as in Moffat (2005a,b); Brownstein & Moffat (2005):

$$G(r) = \left\{ 1 + \sqrt{\frac{M_0}{M_{\text{MSTG}}(r)}} \left[ 1 - \exp(-r/r_0) \left( 1 + \frac{r}{r_0} \right) \right] \right\}. \quad (23)$$

In the limit of large  $r$ , we show in Moffat (2005a,b); Brownstein & Moffat (2005) that

$$G_\infty \equiv \lim_{r \gg r_0} G(r) = G_0 \left\{ 1 + \sqrt{\frac{M_0}{M_{\text{gas}}}} \right\}, \quad (24)$$

and the total mass of the cluster in MSTG can be computed by taking equations (22) to the same limit:

$$\begin{aligned} M_{\text{MSTG}} &= \frac{G_0}{G_\infty} M_N \\ &= \left\{ 1 + \sqrt{\frac{M_0}{M_{\text{MSTG}}}} \right\}^{-1} M_N. \end{aligned} \quad (25)$$

It is a simple matter to solve equations (22) and (25) explicitly for  $M_{\text{MSTG}}(r)$  and  $M_{\text{MSTG}}$ , respectively, by squaring both sides and subsequently applying the canonical solution to the quadratic equation.

The derivation in Milgrom's phenomenological MOND model (Milgrom 1983; Sanders & McGaugh 2002) follows the same procedure, but utilizes the MOND gravitational acceleration law, described by

$$a\mu\left(\frac{a}{a_{0\text{Milgrom}}}\right) = a_{\text{Newton}}, \quad (26)$$

where  $\mu(x)$  is a function that interpolates between the Newtonian regime,  $\mu(x) = 1$ , when  $x \gg 1$  and the MOND regime,  $\mu(x) = x$ , when  $x \ll 1$ . The function and critical acceleration normally used for galaxy and cluster fitting are, respectively,

$$\mu(x) = \frac{x}{\sqrt{1+x^2}}, \quad (27)$$

$$a_{0\text{Milgrom}} = 1.2 \times 10^{-8} \text{ cm/s}^2. \quad (28)$$

Applying equation (26) to either equation (11) or the isothermal case of equation (12) yields the MOND dynamical mass in terms of the Newtonian dynamical mass of equation (18) or the isothermal case of equation (19):

$$M_{\text{MOND}}(r) = \frac{M_N(r)}{\sqrt{1 + (a_{0\text{Milgrom}}/G_0 M_{\text{MOND}}(r)/r^2)^2}}. \quad (29)$$

It is a simple matter to solve equation (29) explicitly for  $M_{\text{MOND}}(r)$  by squaring both sides and subsequently applying the canonical solution to the quadratic equation.

Unlike the Newtonian and MSTG isothermal spheres whose densities fall off as  $1/r^2$  in the limit of large  $r$ , Milgrom (1984) showed that the MOND isothermal spheres have densities that fall off as  $r^{-\alpha}$  where  $\alpha \approx 4$  at large radii. In the Newtonian and MSTG cases, the behavior is Keplerian at large radii and so the isothermal spheres have masses which diverge with  $r$  (Chandrasekhar 1960). Thus according to equations (17) and (20) the acceleration at large radii for Newtonian and MSTG isothermal spheres goes as  $1/r$ . Conversely, the MOND isothermal spheres have convergent masses regardless of the spatial extent Sanders (2003):

$$M_{\text{MOND}} \approx \frac{16}{G_0 a_0 \text{Milgrom}} \left( \frac{kT}{\mu m_p} \right)^2. \quad (30)$$

The MOND acceleration law regularizes the integral of equation (13) whereas a cutoff is necessary in the Newtonian and MSTG case, corresponding to the finite spatial extent of galaxy clusters as shown in equation (16). However, as clearly shown in Sanders (2003), the X-ray surface brightness distribution of these MOND isothermal spheres provides a poor representation of the observed surface brightness distribution. This distinction will become apparent in the section ahead where we study the MSTG and MOND mass profiles of the Coma cluster.

#### 4 RUNNING OF NEWTON'S CONSTANT

We have adopted the compilation of Reiprich (2001); Reiprich & Böhringer (2002) as our sample. The relevant cluster properties are listed in Table 1 arranged as follows: Column (1) lists the cluster name truncated to 8 characters. Column (2) is the observed X-ray temperature. Column (3) lists the ICM central mass density,  $\rho_0$ , of the ICM in units of  $10^{-25} \text{ g/cm}^3$ . Column (4) is the  $\beta$  parameter. Column (5) is the core radius parameter,  $r_c$ , in units of kpc assuming  $H_0 = 0.71_{-0.03}^{+0.04}$  (Eidelman *et al.* 2004). Column (6) is the position,  $r_{\text{out}}$  at which the density,  $\rho(r_{\text{out}})$ , drops to  $\approx 10^{-28} \text{ g/cm}^3$ , or 250 times the mean cosmological density of baryons. Column (7) through (9) lists the ICM gas mass,  $M_{\text{gas}}$ , the Newtonian dynamic mass,  $M_N$ , and the MSTG dynamic mass,  $M_{\text{MSTG}}$ , respectively, each integrated to  $r_{\text{out}}$ . Column (10) lists the ‘‘convergent’’ MOND dynamic mass.

In order to calculate the MSTG dynamic mass we first need to phenomenologically determine the running of the parameters,  $M_0$ , and  $r_0$  – this describes the running of Newton’s constant at the scale of clusters according to equation (23). However, unlike the case of the galaxy rotation curves where a satisfactory fit to LSB and HSB galaxy data is obtained with the parameters (Brownstein & Moffat 2005)

$$M_0 = 9.60 \times 10^{11} M_\odot, \quad r_0 = 13.92 \text{ kpc}, \quad (31)$$

we found that a better fit was attained by dropping the simplifying assumption that  $M_0$  is constant across clusters. In fact, we were able to account for all dwarf galaxies smaller than 12 kpc in Brownstein & Moffat (2005) by allowing  $M_0$  to scale down to:

$$M_0 = 2.40 \times 10^{11} M_\odot, \quad r_0 = 6.96 \text{ kpc}. \quad (32)$$

The three schemes we attempted to prescribe for the scale variation of  $M_0$  for clusters are as follows:

- (i)  $M_0 \propto M_{\text{gas}}^n$ , where  $M_{\text{gas}}$  is the total ICM gas mass integrated to  $r_{\text{out}}$ ,
- (ii)  $M_0 \equiv \text{constant}$ ,
- (iii)  $G_\infty \equiv \text{constant}$ .

It is clear that case (ii) is the limit of case (i) taking  $n \rightarrow 0$  and also that case (iii) is the limit of case (i) taking  $n \rightarrow 1$ . By plotting  $M_N$  against  $M_{\text{gas}}$  and then applying equation (25), we were able to constrain the parameter,  $M_0$ , using a nonlinear least-squares fitting routine including estimated errors. The fits for each of the three above schemes are shown in Figure 1, with the results as follows:

- (i)  $M_0 = (58.8 \pm 4.0) \times 10^{14} M_\odot \left( \frac{M_{\text{gas}}}{10^{14} M_\odot} \right)^{0.39 \pm 0.09}$ ,
- (ii)  $M_0 = (59.4 \pm 4.3) \times 10^{14} M_\odot$ ,
- (iii)  $G_\infty = 7.84 \pm 0.27$ .

The quality of each of these prescriptions for  $M_0$  is seen in their respective plots of Figure 1 where the MSTG mass is plotted against the ICM gas mass. Clearly, the plot corresponding to case (i) is the best scheme since the slope of unity best describes the bulk properties of the clusters. Indeed, the overall least sum of squares best fit is the scheme corresponding to case (i) with the other two acting as limiting cases. Meanwhile, both the MOND ‘‘convergent mass’’ and the Newtonian dynamic mass show a discrepancy with the ICM gas mass (Sanders 2003).

In the galaxy rotation curves, we scaled  $r_0$  down from equation (31) by a factor of 2 to account for the Dwarf galaxies (Brownstein & Moffat 2005). For all but the smallest galaxy clusters where the mass of the ICM dominates over the mass of the individual galaxies, scaling  $r_0$  up from equation (31) by a factor of 10 leads to satisfactory fits, whereas for the smallest galaxy clusters where the mass of the ICM is of the order of galactic masses – with  $r_{\text{out}} \leq 650 \text{ kpc}$  – scaling  $r_0$  to  $r_{\text{out}}/10$  leads to satisfactory fits. Thus our prescription for the running of Newton’s constant (RG flow) for galaxy clusters is fully constrained:

$$M_0 = 58.8 \times 10^{14} M_\odot \left( \frac{M_{\text{gas}}}{10^{14} M_\odot} \right)^{0.39},$$

$$r_0 = r_{\text{out}}/10, \quad r_{\text{out}} \leq 650 \text{ kpc}, \quad (33)$$

$$r_0 = 139.2 \text{ kpc}, \quad r_{\text{out}} > 650 \text{ kpc}.$$

#### 5 INDIVIDUAL CLUSTERS

We now turn to the individual mass profiles for each cluster. Since the MSTG prediction for the mass profile has no free parameters upon enforcing equations (33), we need not perform any nonlinear least-squares fitting for the individual mass profiles as shown in Figure 2. The Coma cluster is shown first (with errorbands); and the remaining 105 clusters follow as thumbnails (without errorbands for clarity).

The  $\beta$ -model is not always a good fit to the data, however, and so the mass profiles shown in Figure 2 have limited reliability and the results of Table 1 show errors ranging from a few percent to in some cases 100%. Ota & Mitsuda (2002) show that some clusters observed with ROSAT and ASCA are expressed better by the double  $\beta$ -model with a second core; while Pointecouteau *et al.* (2005) show that clusters observed with XMM-NEWTON are well described by

an NFW-type profile (Navarro *et al.* 1997) showing strong agreement with CDM simulations. While these more sophisticated mass profile models have their advantages, the simplest isothermal isotropic  $\beta$ -model based upon hydrostatic equilibrium has the fewest parameters and we have used it to show that it is possible and meaningful to fit the X-ray galaxy cluster data without the need for exotic dark matter.

There are also controversial measurements concerning the presence of temperature gradients in galaxy clusters (Reiprich & Böhringer 2002). XMM-NEWTON is expected to probe the isothermal properties of the galaxy clusters. Early results such as the Arnaud *et al.* (2001a) study of the XMM-NEWTON observation of the Coma galaxy cluster and the Arnaud *et al.* (2001b) study of the XMM-NEWTON radial temperature profiles support the isothermal assumption deviating only near the cluster center where the observed X-ray temperatures decrease.

In those cases where the uncertainty in the  $\beta$ -model parameters are sufficiently small (and therefore the  $\beta$ -model provides a suitable fit), the MSTG mass profile traces the ICM gas mass profile down to sufficiently small radii and only deviates where the assumption that the ICM gas mass is isothermal is no longer valid. At sufficiently small radii, the observed X-ray temperatures decrease and thus the MSTG prediction based on an isothermal sphere is too large, confirmed by Figure 2.

## 6 CONCLUSIONS

A gravity theory consisting of a metric-skew-tensor action (MSTG) that leads to the modified acceleration law (Moffat 2005a,b; Brownstein & Moffat 2005) can be fitted to a large class of X-ray galaxy cluster mass profiles. The same acceleration law can also be applied to fit a large class of galaxy rotation curves as in Brownstein & Moffat (2005) – which achieved one parameter fits for the case of the photometric observations with a single parameter  $(M/L)_{\text{stars}}$ ; and also parametric fits which required no simplifying assumption on the constancy of  $(M/L)$  throughout the galaxy. Whereas MOND provides a good phenomenological fit to galaxy rotation curves, only MSTG fits both galaxy rotation curves and the X-ray galaxy cluster mass profiles without the need of introducing a non-baryonic dark matter component.

In addition, whereas MOND necessitates the asymptotic “flat rotation” velocity out to infinity, MSTG only gives the appearance of a “flat rotation” velocity within the confines of the galaxy and returns to the familiar Newton-Kepler form at large distances. Using the Sloan Digital Sky Survey (SDSS), Prada *et al.* (2003) have studied the velocities of satellites orbiting isolated galaxies. They detected approximately 3000 satellites, and they found that the line-of-sight velocity dispersion of satellites declines with distance to the primary. The velocity was observed to decline to a distance of  $\sim 350$  kpc for the available data. This result contradicts the constant velocity prediction equation of MOND, but is consistent with the MSTG prediction.

The newest results from XMM-NEWTON reveal that the mass profiles of X-ray clusters show a steady rise out to the limit of X-ray observations (Pointecouteau *et al.* 2005) and do not show the convergent behavior of MOND isothermal spheres. However, the XMM-NEWTON results are consistent

with the MSTG isothermal sphere whose densities fall off as  $1/r^2$  without unseen non-baryonic dark matter. Further results from XMM-NEWTON may reveal that the temperature profiles of X-ray clusters are not everywhere isothermal; and observed gradients may add a greater understanding of the physics of X-ray clusters of galaxies and the law of gravitation that best describes these largest of virialized objects.

## ACKNOWLEDGMENTS

This work was supported by the Natural Sciences and Engineering Research Council of Canada. We thank Thomas H. Reiprich for supplying the data for our galaxy cluster sample via [electronic table](#)<sup>1</sup>.

## REFERENCES

- Aguirre, A., Schaye, J. & Quataert, E. 2001, ApJ, 561, 550  
 Arnaud, M. *et al.* 2001, A&A, 365, L67  
 Arnaud, M., Neumann D. M., Aghanim, N., Gastaud, R., Majerowicz, S. & Hughes, J. P. 2001, A&A, 365, L80  
 Brownstein, J. R. & Moffat, J. W. 2005, ApJ, submitted ([astro-ph/0506370](#))  
 Cavaliere, A. L. & Fusco-Femiano, R. 1976, A&A, 49, 137  
 Chandrasekhar, S. 1960, *Principles of Stellar Dynamics*, Dover, New York  
 Eidelman, S. *et al.* 2004, Phys. Lett. B592, 1, 2005 update (<http://pdg.lbl.gov>)  
 King, I. R. 1966, AJ, 71, 64  
 Milgrom, M. 1983, ApJ, 270, 365  
 Milgrom, M. 1983, ApJ, 287, 571  
 Moffat, J. W. 2005, J. Cosmology Astropart. Phys., 05, 003  
 Moffat, J. W. 2005, preprint ([gr-qc/0506021](#))  
 Navarro, J. F., Frenk, C. S., & White, S. D. M. 1997, ApJ, 490, 493  
 Ota, N. & Mitsuda, K. 2002, ApJ, 567, L23  
 Pointecouteau, E., Arnaud, M. & Pratt, G. W. 2005, A&A, 435, 1  
 Pointecouteau, E. & Silk, J. 2005, MNRAS, submitted ([astro-ph/0505017](#))  
 Prada, F. *et al.* 2003, ApJ, 598, 260  
 Reiprich, T. H. 2001, Ph.D. Dissertation, *Cosmological Implications and Physical Properties of an X-Ray Flux-Limited Sample of Galaxy Clusters*, Ludwig-Maximilians-Universität München  
 Reiprich, T. H. & Böhringer, H. 2002, ApJ, 567, 716  
 Reuter, M. & Weyer, H. 2004, J. Cosmology Astropart. Phys., 12, 001  
 Reuter, M. & Weyer, H. 2004, Phys. Rev. D69, 104022  
 Sanders, R. H. 2003, MNRAS, 342, 901  
 Sanders, R. H. & McGaugh, S. S. 2002, ARA&A40, 263  
 The L. S. & White S. D. M. 1988, AJ, 95, 1642  
 Zwicky, F. 1933, Helv. Phys. Acta., 6, 110

<sup>1</sup> <http://www.astro.virginia.edu/~thr4f/act/gcs/>

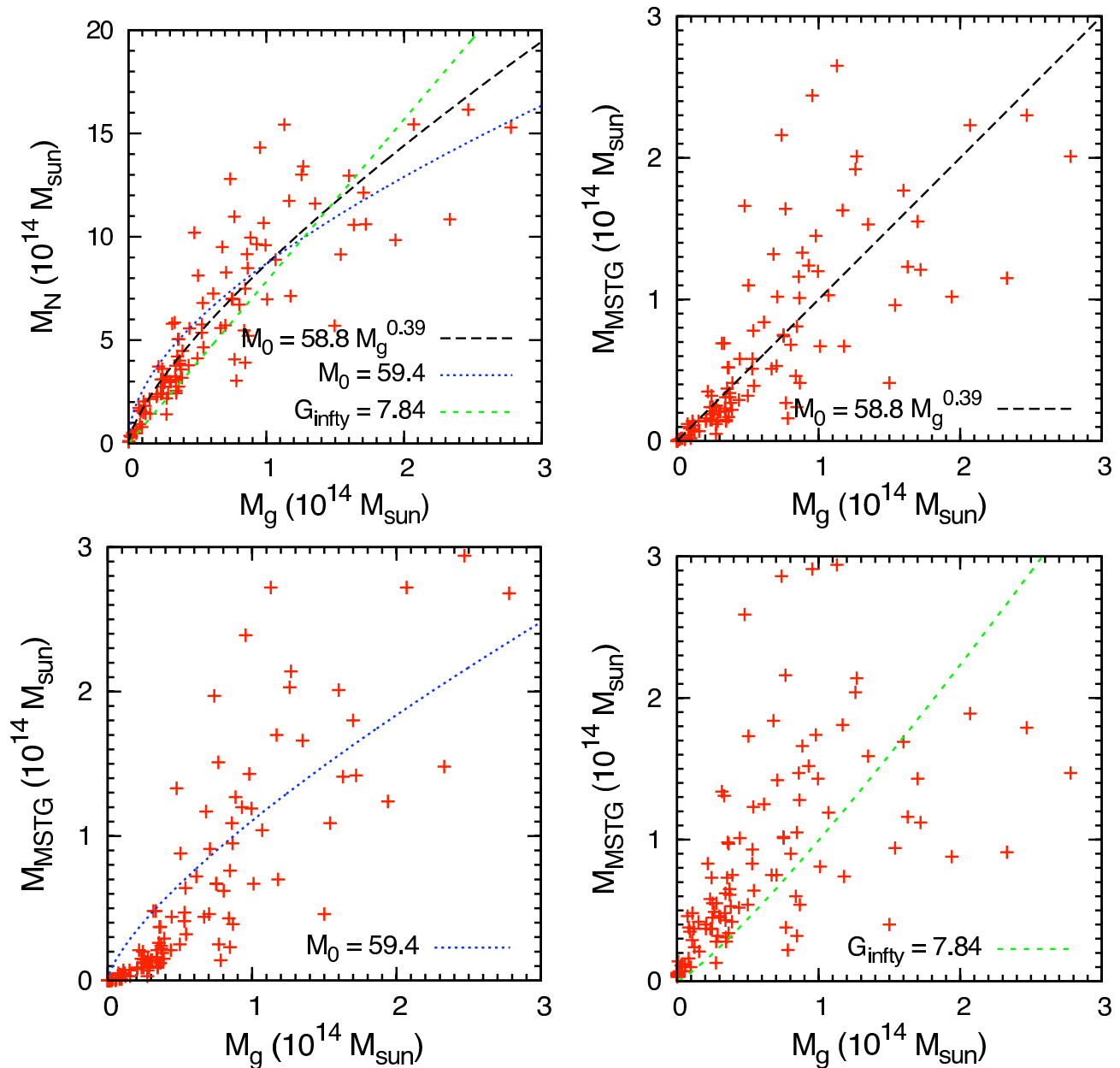


**Figure 1.** A plot of the observed masses of the galaxy clusters in our sample listed in Table 1 versus the inferred Newtonian dynamic masses of the galaxy clusters and the best fit MSTG dynamic masses renormalized by three different schemes across all galaxy clusters: (1)  $M_0 \propto M_{\text{gas}}^a$ , where  $M_{\text{gas}}$  is the total mass of the cluster (black long dashed curve), (2)  $M_0 \equiv \text{constant}$  (blue dotted curve), and (3)  $G_\infty \equiv \text{constant}$  (green short dashed curve). Red + -points are individual clusters from  $\beta$ -model data (Reiprich 2001; Reiprich & Böhringer 2002). The MSTG dynamic mass in these three schemes is plotted in the remaining three graphs. Scheme (1) leads to the smallest sum of squares and is the overall best fit to the data with  $M_0 \approx 58.8 M_{\text{gas}}^{0.39} [10^{14} M_\odot]$ . Scheme (2) is an acceptable fit of the bulk properties with  $M_0 \approx 59.4 \times 10^{14} M_\odot$ . Scheme (3) is a marginal fit of the bulk properties with  $G_\infty \approx 7.84 G_0$ . Both dynamic masses,  $M_{\text{MSTG}}$  and  $M_N$  are computed for isotropic, isothermal spheres cutoff at a spatial extent corresponding to a density of  $10^{-28} \text{ g/cm}^3$ . Error bars are omitted for clarity – the computed errors are provided in Table 1 for completeness.

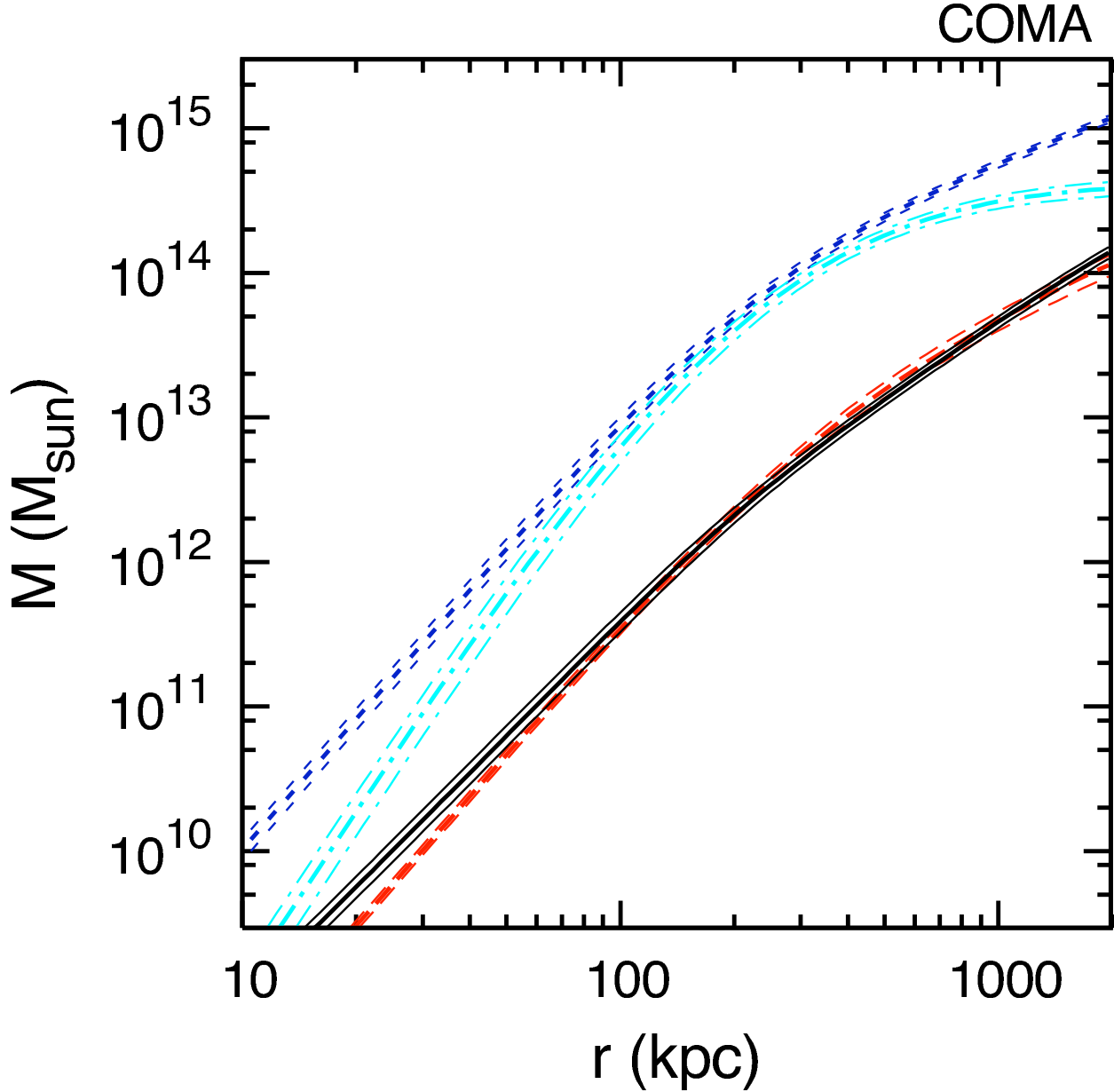


**Figure 2.** Galaxy Cluster Mass Profiles: Plot of the radial mass profile for the 106 clusters in the sample of Table 1. In all cases, the horizontal axis is the radius in kpc and the vertical axis is mass in units of  $10^{14} M_{\odot}$ . The red long dashed curve is the ICM gas mass inferred from X-ray observations according to the compilation of Reiprich (2001); Reiprich & Böhringer (2002); the short dashed blue curve is the Newtonian dynamic mass; the dashed-dotted cyan curve is the MOND dynamic mass; and the solid black curve is the MSTG dynamic mass. The Newtonian, MOND and MSTG dynamic masses are calculated within the context of the  $\beta$ -model isothermal, isotropic sphere. The uncertainty in  $T$ ,  $\beta$ ,  $r_c$  and  $H_0$  is shown for the COMA cluster as a representative case of a cluster with a well fit  $\beta$ -model; but error bands are omitted in the subsequent thumbnail plots for clarity.

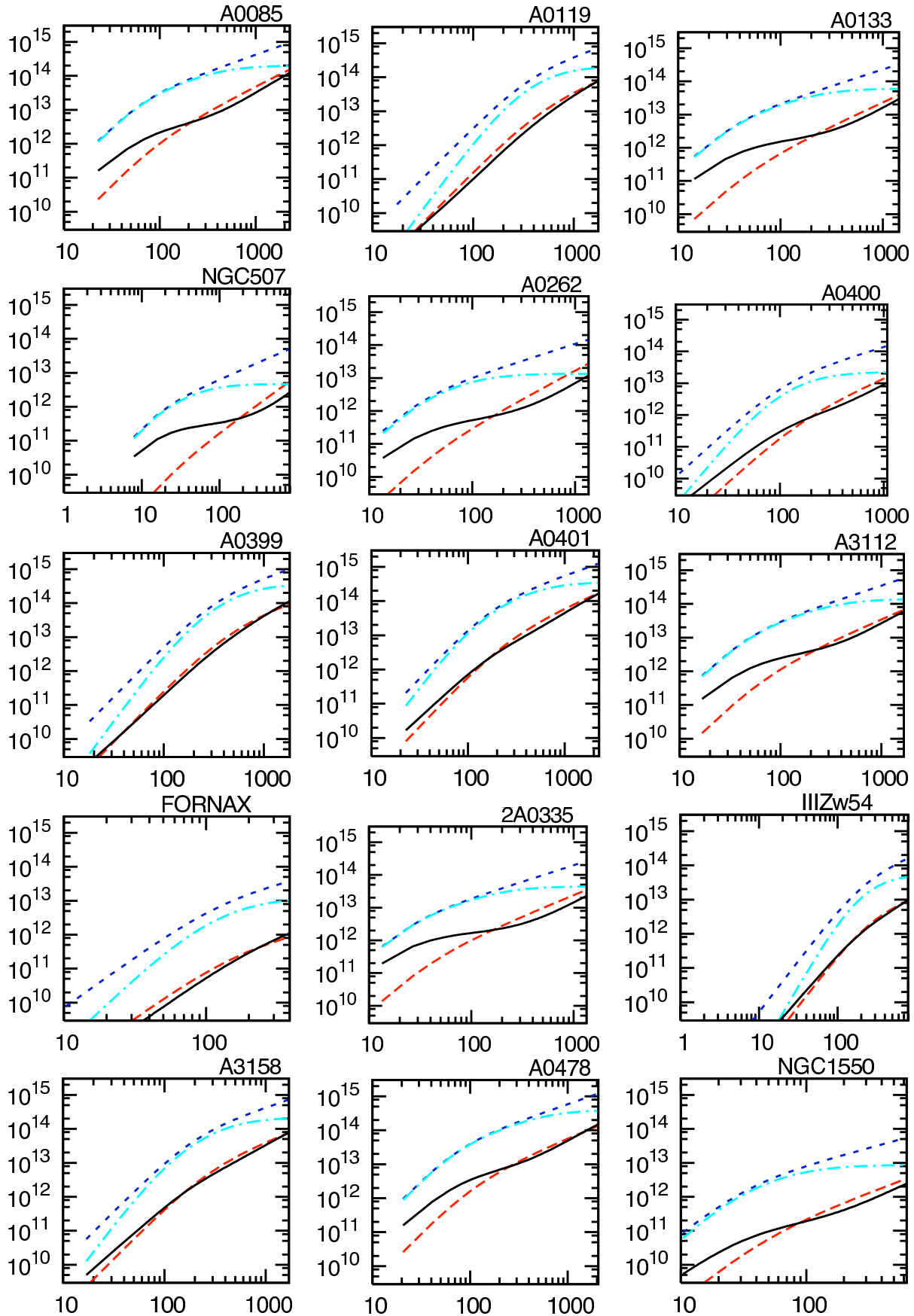


Figure 2 – *continued* Galaxy Cluster Mass Profiles



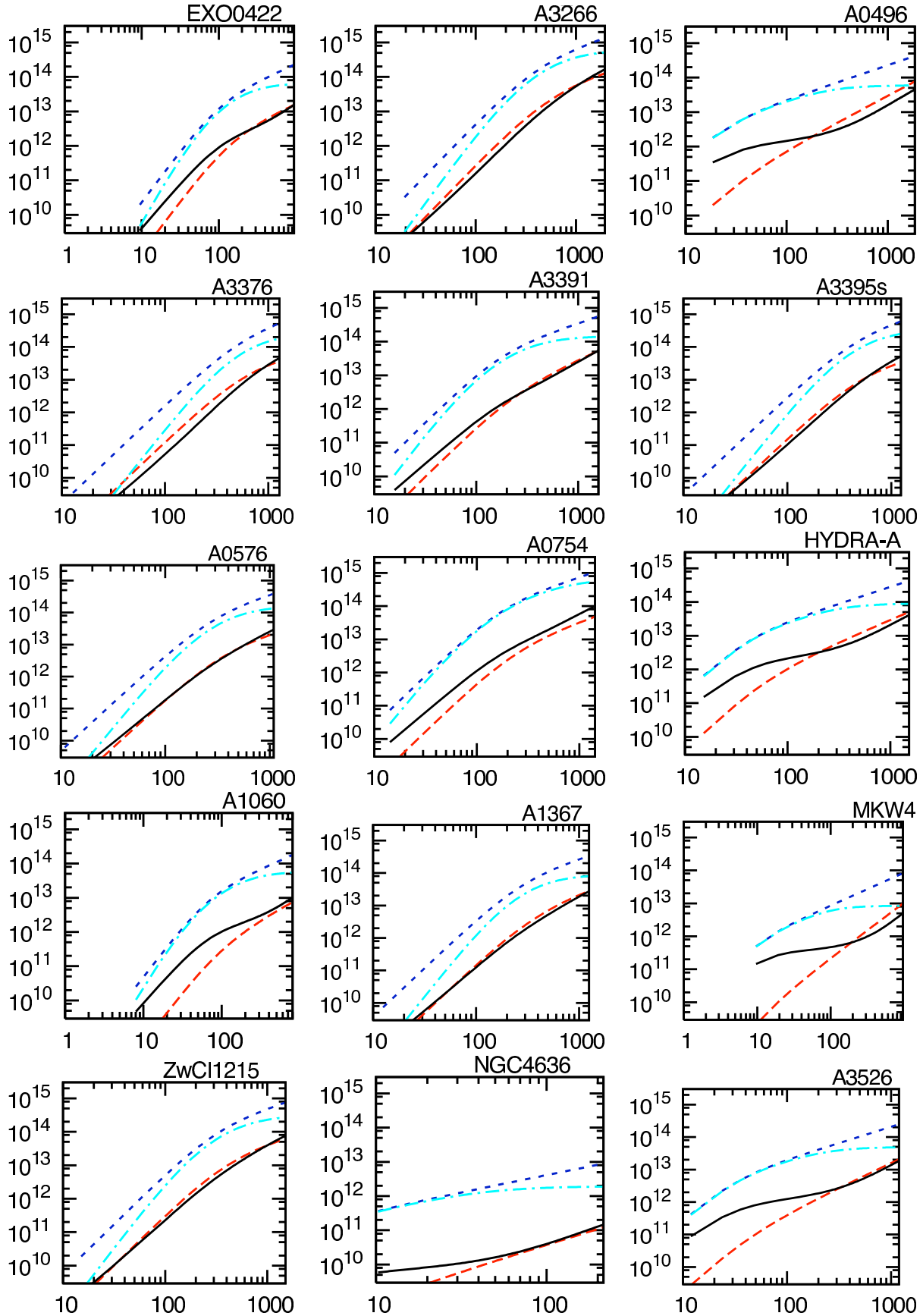


Figure 2 – continued Galaxy Cluster Mass Profiles

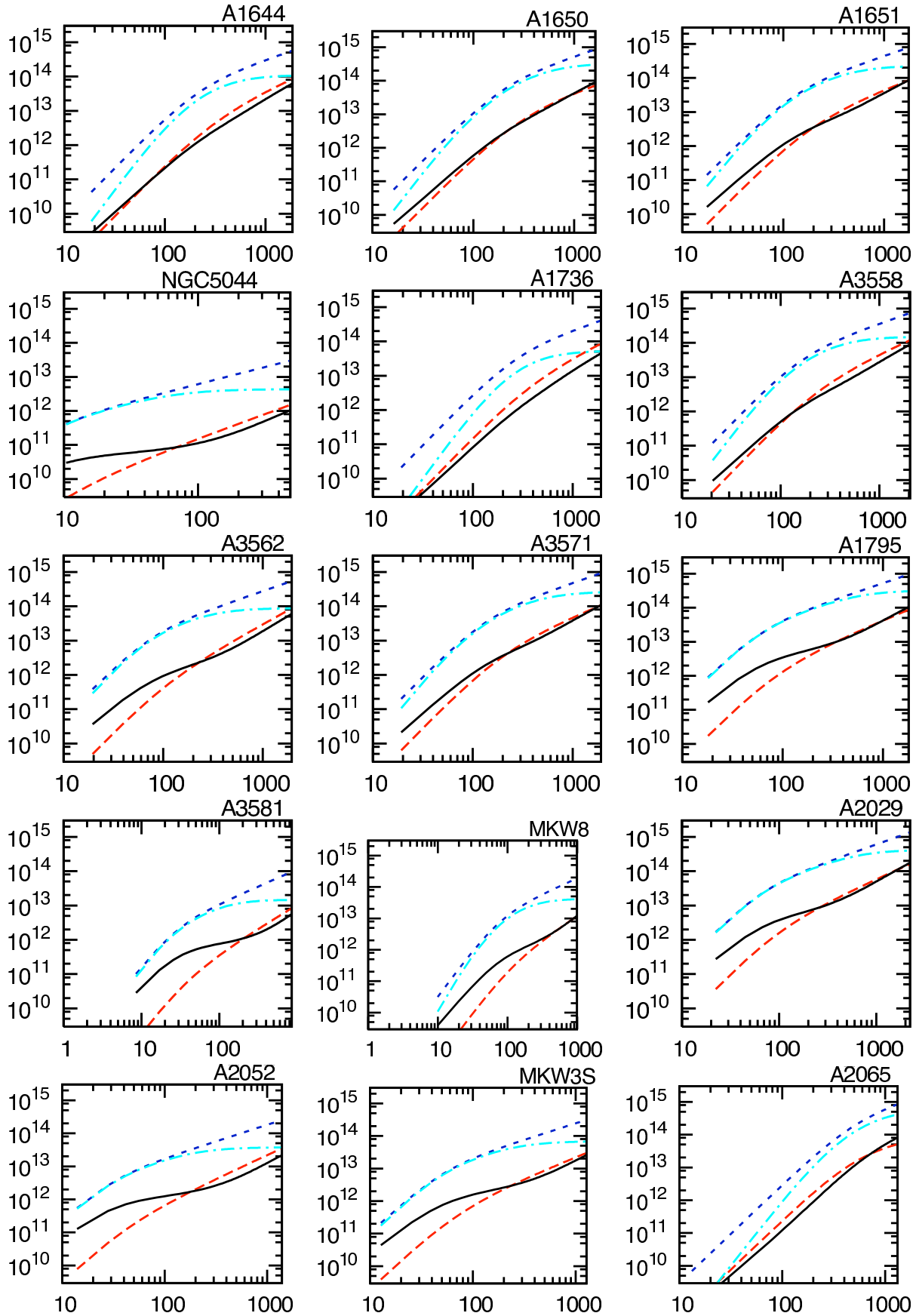


Figure 2 – *continued* Galaxy Cluster Mass Profiles

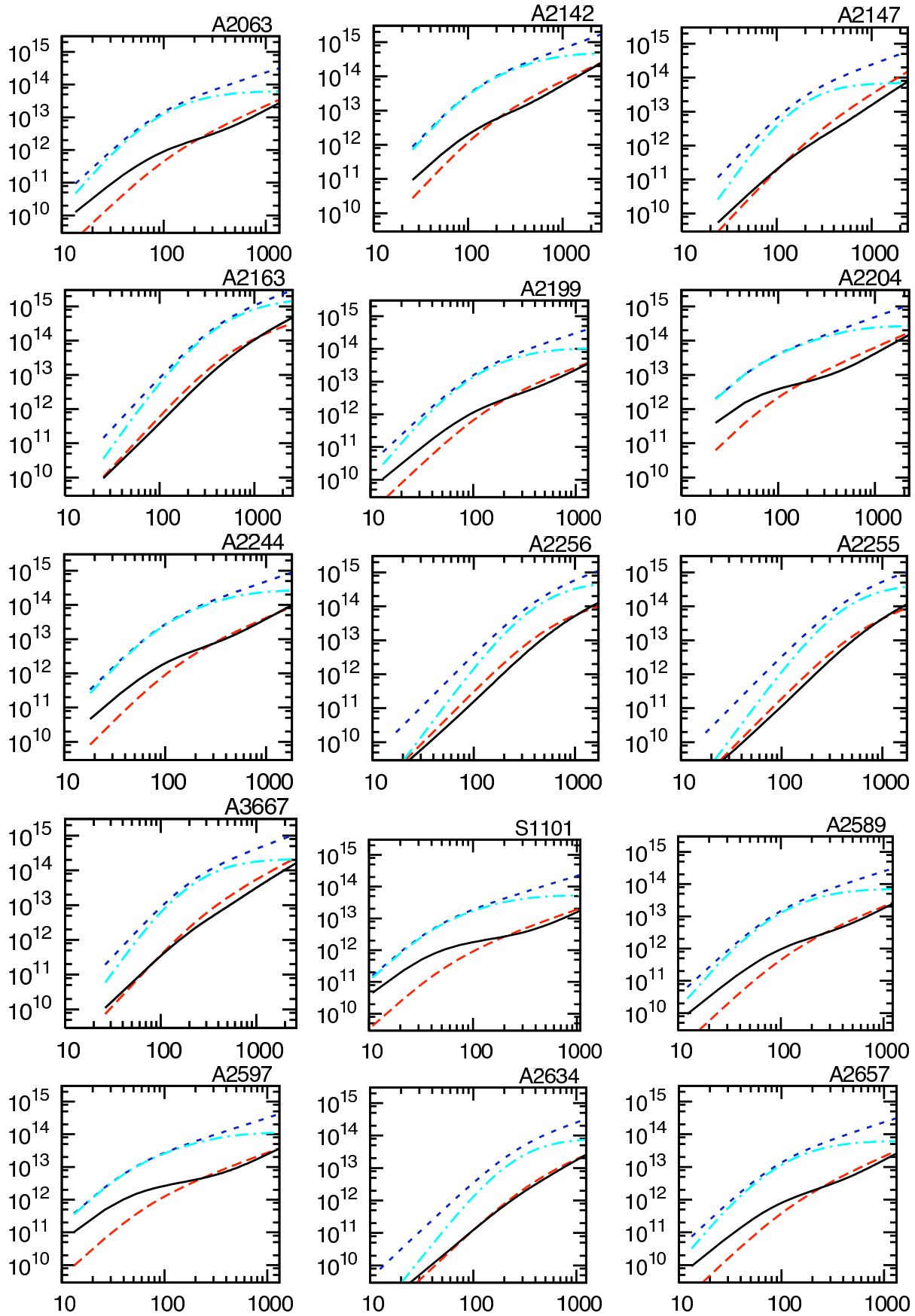


Figure 2 – continued Galaxy Cluster Mass Profiles

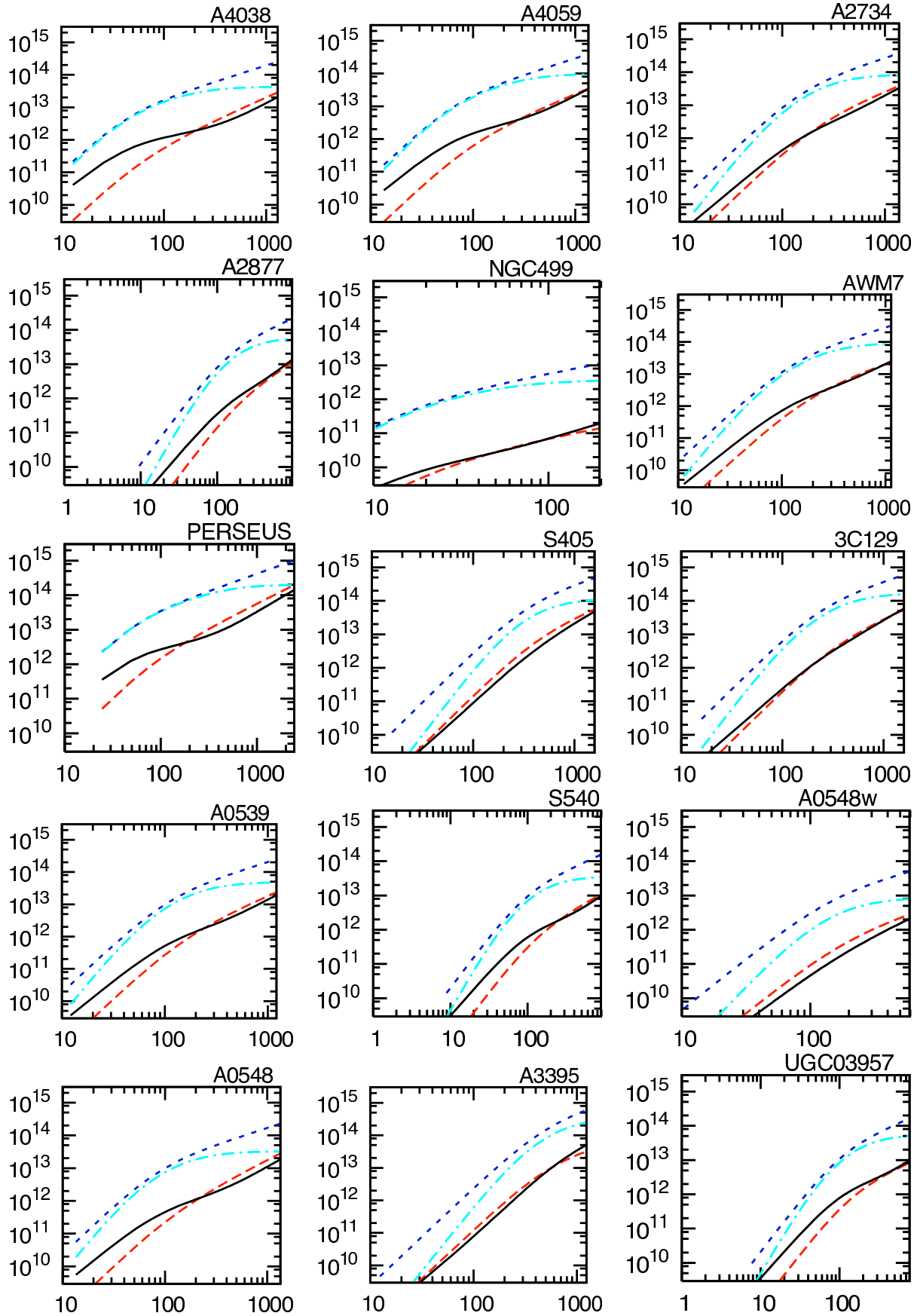


Figure 2 – *continued* Galaxy Cluster Mass Profiles

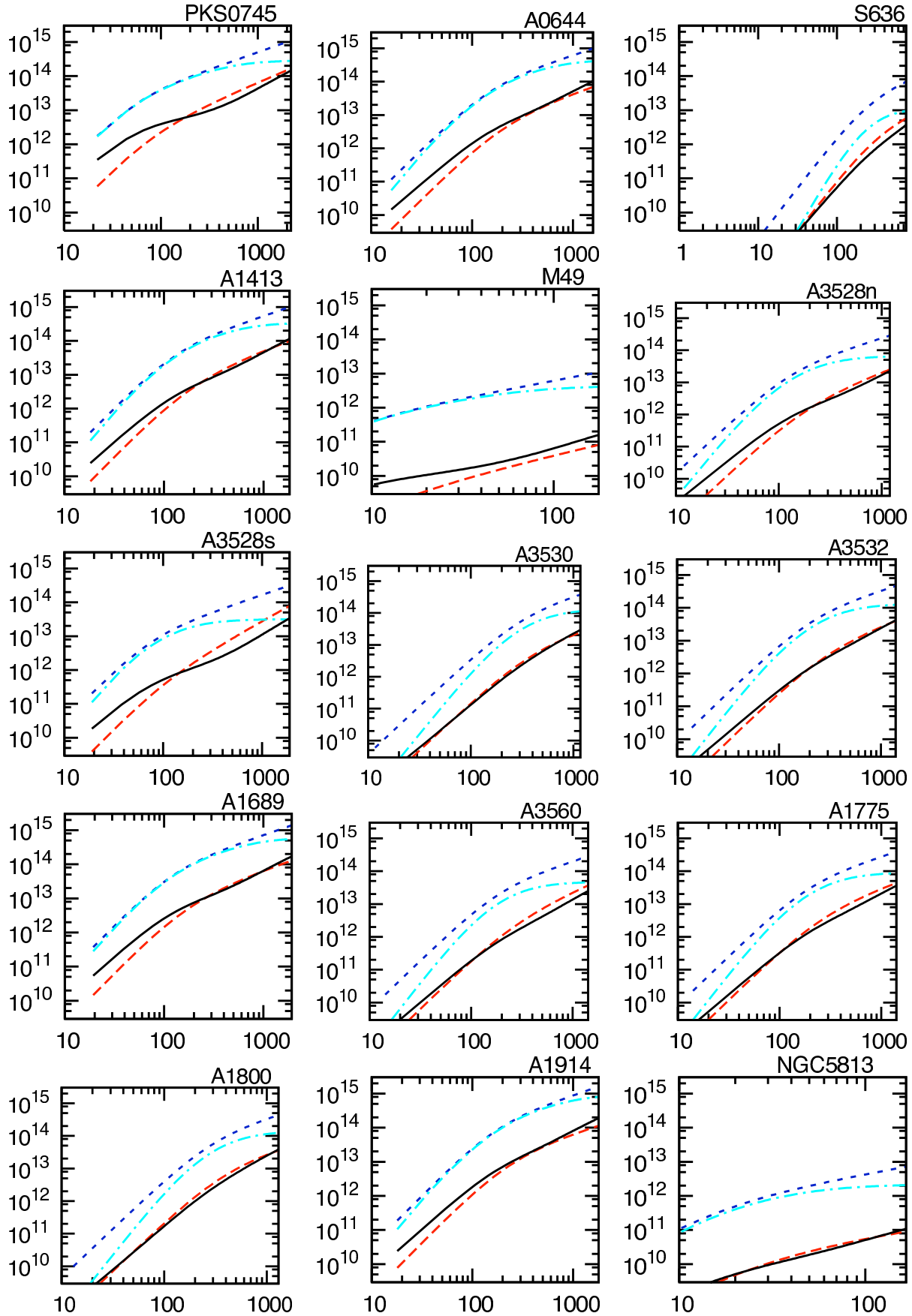


Figure 2 – continued Galaxy Cluster Mass Profiles

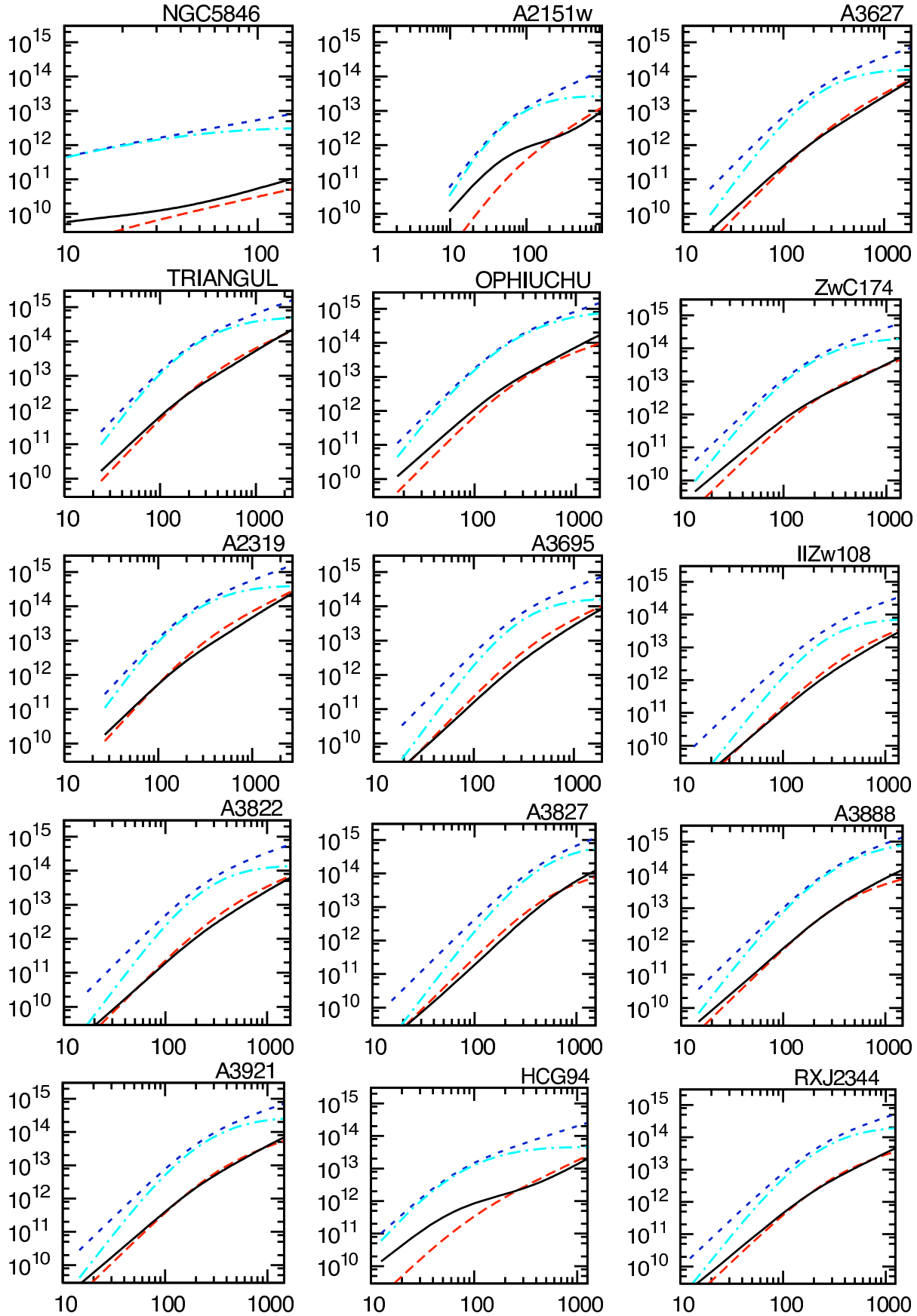


Figure 2 – *continued* Galaxy Cluster Mass Profiles

Table 1. X-RAY CLUSTER PROPERTIES OF THE Complete Sample:

Cluster	$T$ [keV]	$\rho_0$ [ $10^{-25}$ g/cm $^3$ ]	$\beta$	$r_c$ [kpc]	$r_{out}$ [kpc]	$M_{gas}$ [ $10^{14} M_{\odot}$ ]	$M_N$ [ $10^{14} M_{\odot}$ ]	$M_{MSTG}$ [ $10^{14} M_{\odot}$ ]	$M_{MOND}$ [ $10^{14} M_{\odot}$ ]
(1)	(2)	(3)	(4)	(5)	(6)	(7)	(8)	(9)	(10)
A0085	6.90 <sup>+0.40</sup> <sub>-0.40</sub>	0.34	0.532 <sup>+0.004</sup> <sub>-0.004</sub>	58.5 <sup>+3.3</sup> <sub>-3.2</sub>	2, 241 <sup>+139</sup> <sub>-162</sub>	1.48 <sup>+0.14</sup> <sub>-0.16</sub>	9.02 <sup>+0.53</sup> <sub>-0.53</sub>	1.15 <sup>+0.08</sup> <sub>-0.09</sub>	1.83 <sup>+0.21</sup> <sub>-0.21</sub>
A0119	5.60 <sup>+0.30</sup> <sub>-0.30</sub>	0.03	0.675 <sup>+0.026</sup> <sub>-0.023</sub>	352.8 <sup>+24.7</sup> <sub>-27.0</sub>	1, 728 <sup>+163</sup> <sub>-173</sub>	0.73 <sup>+0.10</sup> <sub>-0.10</sub>	6.88 <sup>+0.83</sup> <sub>-0.50</sub>	0.73 <sup>+0.07</sup> <sub>-0.07</sub>	1.76 <sup>+0.26</sup> <sub>-0.25</sub>
A0133	3.80 <sup>+2.00</sup> <sub>-0.90</sub>	0.42	0.530 <sup>+0.004</sup> <sub>-0.004</sub>	31.7 <sup>+1.9</sup> <sub>-2.3</sub>	1, 417 <sup>+96</sup> <sub>-109</sub>	0.37 <sup>+0.04</sup> <sub>-0.04</sub>	3.13 <sup>+1.65</sup> <sub>-0.74</sub>	0.28 <sup>+0.15</sup> <sub>-0.07</sub>	0.55 <sup>+0.57</sup> <sub>-0.26</sub>
NGC507	1.26 <sup>+0.07</sup> <sub>-0.07</sub>	0.23	0.444 <sup>+0.005</sup> <sub>-0.005</sub>	13.4 <sup>+0.9</sup> <sub>-1.0</sub>	783 <sup>+64</sup> <sub>-70</sub>	0.05 <sup>+0.01</sup> <sub>-0.01</sub>	0.48 <sup>+0.03</sup> <sub>-0.03</sub>	0.02 <sup>+0.00</sup> <sub>-0.00</sub>	0.04 <sup>+0.00</sup> <sub>-0.00</sub>
A0262	2.15 <sup>+0.06</sup> <sub>-0.06</sub>	0.16	0.443 <sup>+0.018</sup> <sub>-0.017</sub>	29.6 <sup>+8.5</sup> <sub>-7.2</sub>	1, 334 <sup>+432</sup> <sub>-386</sub>	0.26 <sup>+0.11</sup> <sub>-0.10</sub>	1.39 <sup>+0.09</sup> <sub>-0.09</sub>	0.11 <sup>+0.02</sup> <sub>-0.02</sub>	0.13 <sup>+0.02</sup> <sub>-0.02</sub>
A0400	2.31 <sup>+0.14</sup> <sub>-0.14</sub>	0.04	0.534 <sup>+0.014</sup> <sub>-0.013</sub>	108.5 <sup>+7.8</sup> <sub>-8.8</sub>	1, 062 <sup>+97</sup> <sub>-108</sub>	0.15 <sup>+0.02</sup> <sub>-0.02</sub>	1.42 <sup>+0.10</sup> <sub>-0.10</sub>	0.10 <sup>+0.01</sup> <sub>-0.01</sub>	0.20 <sup>+0.03</sup> <sub>-0.03</sub>
A0399	7.00 <sup>+0.40</sup> <sub>-0.40</sub>	0.04	0.713 <sup>+0.137</sup> <sub>-0.095</sub>	316.9 <sup>+93.9</sup> <sub>-72.7</sub>	1, 791 <sup>+683</sup> <sub>-774</sub>	0.90 <sup>+0.35</sup> <sub>-0.48</sub>	9.51 <sup>+2.64</sup> <sub>-1.64</sub>	1.07 <sup>+0.41</sup> <sub>-0.33</sub>	3.07 <sup>+1.62</sup> <sub>-1.15</sub>
A0401	8.00 <sup>+0.40</sup> <sub>-0.40</sub>	0.11	0.613 <sup>+0.010</sup> <sub>-0.010</sub>	173.2 <sup>+10.7</sup> <sub>-12.0</sub>	2, 236 <sup>+167</sup> <sub>-182</sub>	1.65 <sup>+0.20</sup> <sub>-0.22</sub>	11.96 <sup>+0.66</sup> <sub>-0.66</sub>	1.58 <sup>+0.12</sup> <sub>-0.13</sub>	3.18 <sup>+0.34</sup> <sub>-0.34</sub>
A3112	5.30 <sup>+0.70</sup> <sub>-1.00</sub>	0.54	0.576 <sup>+0.006</sup> <sub>-0.006</sub>	43.0 <sup>+2.8</sup> <sub>-3.2</sub>	1, 644 <sup>+124</sup> <sub>-138</sub>	0.64 <sup>+0.08</sup> <sub>-0.09</sub>	5.50 <sup>+0.73</sup> <sub>-1.04</sub>	0.56 <sup>+0.08</sup> <sub>-0.11</sub>	1.26 <sup>+0.33</sup> <sub>-0.46</sub>
FORNAX	1.20 <sup>+0.04</sup> <sub>-0.04</sub>	0.02	0.804 <sup>+0.098</sup> <sub>-0.084</sub>	122.5 <sup>+13.0</sup> <sub>-12.6</sub>	387 <sup>+67</sup> <sub>-74</sub>	0.009 <sup>+0.004</sup> <sub>-0.003</sub>	0.373 <sup>+0.066</sup> <sub>-0.057</sub>	0.11 <sup>+0.003</sup> <sub>-0.003</sub>	0.102 <sup>+0.035</sup> <sub>-0.030</sub>
2A0335	3.01 <sup>+0.07</sup> <sub>-0.07</sub>	1.07	0.575 <sup>+0.004</sup> <sub>-0.003</sub>	23.2 <sup>+1.2</sup> <sub>-1.5</sub>	1, 322 <sup>+74</sup> <sub>-92</sub>	0.33 <sup>+0.03</sup> <sub>-0.04</sub>	2.51 <sup>+0.06</sup> <sub>-0.06</sub>	0.21 <sup>+0.01</sup> <sub>-0.01</sub>	0.41 <sup>+0.02</sup> <sub>-0.02</sub>
IIIZw54	2.16 <sup>+0.35</sup> <sub>-0.30</sub>	0.04	0.887 <sup>+0.320</sup> <sub>-0.151</sub>	203.5 <sup>+87.7</sup> <sub>-52.7</sub>	780 <sup>+389</sup> <sub>-461</sub>	0.09 <sup>+0.09</sup> <sub>-0.09</sub>	1.54 <sup>+0.82</sup> <sub>-0.43</sub>	0.09 <sup>+0.09</sup> <sub>-0.09</sub>	0.43 <sup>+0.44</sup> <sub>-0.23</sub>
A3158	5.77 <sup>+0.10</sup> <sub>-0.05</sub>	0.08	0.661 <sup>+0.022</sup> <sub>-0.022</sub>	189.4 <sup>+18.2</sup> <sub>-17.1</sub>	1, 672 <sup>+189</sup> <sub>-206</sub>	0.73 <sup>+0.13</sup> <sub>-0.14</sub>	6.91 <sup>+0.39</sup> <sub>-0.33</sub>	0.73 <sup>+0.07</sup> <sub>-0.07</sub>	1.89 <sup>+0.20</sup> <sub>-0.17</sub>
A0478	8.40 <sup>+0.80</sup> <sub>-1.40</sub>	0.5	0.613 <sup>+0.004</sup> <sub>-0.004</sub>	69.0 <sup>+3.2</sup> <sub>-4.1</sub>	2, 029 <sup>+105</sup> <sub>-130</sub>	1.30 <sup>+0.12</sup> <sub>-0.15</sub>	11.45 <sup>+1.10</sup> <sub>-1.91</sub>	1.42 <sup>+0.15</sup> <sub>-0.25</sub>	3.49 <sup>+0.64</sup> <sub>-1.11</sub>
NGC1550	1.43 <sup>+0.04</sup> <sub>-0.03</sub>	0.15	0.554 <sup>+0.049</sup> <sub>-0.037</sub>	31.7 <sup>+10.6</sup> <sub>-7.9</sub>	632 <sup>+247</sup> <sub>-231</sub>	0.034 <sup>+0.020</sup> <sub>-0.018</sub>	0.548 <sup>+0.070</sup> <sub>-0.053</sub>	0.024 <sup>+0.007</sup> <sub>-0.007</sub>	0.086 <sup>+0.022</sup> <sub>-0.016</sub>
EXO0422	2.90 <sup>+0.90</sup> <sub>-0.60</sub>	0.13	0.722 <sup>+0.104</sup> <sub>-0.071</sub>	100.0 <sup>+28.5</sup> <sub>-21.9</sub>	934 <sup>+338</sup> <sub>-367</sub>	0.15 <sup>+0.09</sup> <sub>-0.09</sub>	2.12 <sup>+0.79</sup> <sub>-0.53</sub>	0.14 <sup>+0.07</sup> <sub>-0.05</sub>	0.57 <sup>+0.41</sup> <sub>-0.27</sub>
A3266	8.00 <sup>+0.50</sup> <sub>-0.50</sub>	0.05	0.796 <sup>+0.020</sup> <sub>-0.019</sub>	397.2 <sup>+22.4</sup> <sub>-26.4</sub>	1, 915 <sup>+132</sup> <sub>-150</sub>	1.22 <sup>+0.13</sup> <sub>-0.16</sub>	12.82 <sup>+0.92</sup> <sub>-0.91</sub>	1.56 <sup>+0.13</sup> <sub>-0.14</sub>	4.79 <sup>+0.64</sup> <sub>-0.63</sub>
A0496	4.13 <sup>+0.08</sup> <sub>-0.08</sub>	0.65	0.484 <sup>+0.003</sup> <sub>-0.003</sub>	21.1 <sup>+1.1</sup> <sub>-1.4</sub>	1, 830 <sup>+111</sup> <sub>-130</sub>	0.74 <sup>+0.06</sup> <sub>-0.07</sub>	4.01 <sup>+0.09</sup> <sub>-0.09</sub>	0.43 <sup>+0.02</sup> <sub>-0.02</sub>	0.55 <sup>+0.02</sup> <sub>-0.02</sub>
A3376	4.00 <sup>+0.40</sup> <sub>-0.40</sub>	0.02	1.054 <sup>+0.101</sup> <sub>-0.083</sub>	531.7 <sup>+53.5</sup> <sub>-51.8</sub>	1, 264 <sup>+169</sup> <sub>-183</sub>	0.35 <sup>+0.35</sup> <sub>-0.35</sub>	4.97 <sup>+0.85</sup> <sub>-0.76</sub>	0.43 <sup>+0.43</sup> <sub>-0.43</sub>	1.67 <sup>+0.54</sup> <sub>-0.48</sub>
A3391	5.40 <sup>+0.60</sup> <sub>-0.60</sub>	0.05	0.579 <sup>+0.026</sup> <sub>-0.024</sub>	164.8 <sup>+18.3</sup> <sub>-18.1</sub>	1, 558 <sup>+227</sup> <sub>-234</sub>	0.51 <sup>+0.11</sup> <sub>-0.11</sub>	5.28 <sup>+0.68</sup> <sub>-0.66</sub>	0.51 <sup>+0.08</sup> <sub>-0.08</sub>	1.29 <sup>+0.32</sup> <sub>-0.31</sub>
A3395s	5.00 <sup>+0.30</sup> <sub>-0.30</sub>	0.03	0.964 <sup>+0.275</sup> <sub>-0.167</sub>	425.4 <sup>+123.1</sup> <sub>-86.5</sub>	1, 223 <sup>+442</sup> <sub>-501</sub>	0.32 <sup>+0.32</sup> <sub>-0.32</sub>	5.77 <sup>+2.37</sup> <sub>-1.50</sub>	0.49 <sup>+0.49</sup> <sub>-0.49</sub>	2.34 <sup>+1.76</sup> <sub>-1.12</sub>
A0576	4.02 <sup>+0.07</sup> <sub>-0.07</sub>	0.03	0.825 <sup>+0.432</sup> <sub>-0.185</sub>	277.5 <sup>+156.1</sup> <sub>-89.4</sub>	1, 076 <sup>+703</sup> <sub>-903</sub>	0.21 <sup>+0.41</sup> <sub>-0.19</sub>	3.67 <sup>+2.72</sup> <sub>-1.19</sub>	0.28 <sup>+0.32</sup> <sub>-0.15</sub>	1.26 <sup>+1.76</sup> <sub>-0.77</sub>
A0754	9.50 <sup>+0.70</sup> <sub>-0.40</sub>	0.09	0.698 <sup>+0.027</sup> <sub>-0.024</sub>	168.3 <sup>+13.9</sup> <sub>-14.7</sub>	1, 402 <sup>+156</sup> <sub>-170</sub>	0.46 <sup>+0.08</sup> <sub>-0.09</sub>	10.05 <sup>+0.92</sup> <sub>-0.65</sub>	0.94 <sup>+0.12</sup> <sub>-0.10</sub>	5.10 <sup>+0.82</sup> <sub>-0.57</sub>
HYDRA-A	4.30 <sup>+0.40</sup> <sub>-0.40</sub>	0.63	0.573 <sup>+0.003</sup> <sub>-0.003</sub>	35.2 <sup>+1.6</sup> <sub>-2.1</sub>	1, 502 <sup>+76</sup> <sub>-95</sub>	0.49 <sup>+0.04</sup> <sub>-0.05</sub>	4.06 <sup>+0.38</sup> <sub>-0.38</sub>	0.38 <sup>+0.04</sup> <sub>-0.04</sub>	0.82 <sup>+0.15</sup> <sub>-0.15</sub>
A1060	3.24 <sup>+0.06</sup> <sub>-0.06</sub>	0.09	0.607 <sup>+0.040</sup> <sub>-0.034</sub>	66.2 <sup>+10.9</sup> <sub>-9.9</sub>	790 <sup>+171</sup> <sub>-176</sub>	0.07 <sup>+0.02</sup> <sub>-0.02</sub>	1.69 <sup>+0.16</sup> <sub>-0.14</sub>	0.10 <sup>+0.02</sup> <sub>-0.02</sub>	0.50 <sup>+0.09</sup> <sub>-0.08</sub>
A1367	3.55 <sup>+0.08</sup> <sub>-0.08</sub>	0.03	0.695 <sup>+0.035</sup> <sub>-0.032</sub>	269.7 <sup>+20.4</sup> <sub>-21.7</sub>	1, 234 <sup>+131</sup> <sub>-141</sub>	0.27 <sup>+0.04</sup> <sub>-0.04</sub>	3.19 <sup>+0.24</sup> <sub>-0.22</sub>	0.26 <sup>+0.03</sup> <sub>-0.03</sub>	0.75 <sup>+0.11</sup> <sub>-0.10</sub>
MKW4	1.71 <sup>+0.09</sup> <sub>-0.09</sub>	0.57	0.440 <sup>+0.004</sup> <sub>-0.005</sub>	7.7 <sup>+0.8</sup> <sub>-0.8</sub>	948 <sup>+108</sup> <sub>-110</sub>	0.09 <sup>+0.01</sup> <sub>-0.01</sub>	0.78 <sup>+0.04</sup> <sub>-0.04</sub>	0.05 <sup>+0.00</sup> <sub>-0.00</sub>	0.08 <sup>+0.01</sup> <sub>-0.01</sub>
ZwCl1215	5.58 <sup>+0.89</sup> <sub>-0.78</sub>	0.05	0.819 <sup>+0.038</sup> <sub>-0.034</sub>	303.5 <sup>+23.5</sup> <sub>-24.5</sub>	1, 485 <sup>+155</sup> <sub>-167</sub>	0.59 <sup>+0.10</sup> <sub>-0.10</sub>	7.15 <sup>+1.23</sup> <sub>-1.08</sub>	0.72 <sup>+0.13</sup> <sub>-0.12</sub>	2.50 <sup>+0.81</sup> <sub>-0.71</sub>
NGC4636	0.76 <sup>+0.01</sup> <sub>-0.01</sub>	0.33	0.491 <sup>+0.032</sup> <sub>-0.027</sub>	4.2 <sup>+1.4</sup> <sub>-1.4</sub>	216 <sup>+118</sup> <sub>-92</sub>	0.01 <sup>+0.01</sup> <sub>-0.01</sub>	0.088 <sup>+0.008</sup> <sub>-0.007</sub>	0.01 <sup>+0.01</sup> <sub>-0.01</sub>	0.19 <sup>+0.03</sup> <sub>-0.03</sub>
A3526	3.68 <sup>+0.06</sup> <sub>-0.06</sub>	0.29	0.495 <sup>+0.011</sup> <sub>-0.010</sub>	26.1 <sup>+3.7</sup> <sub>-3.2</sub>	1, 175 <sup>+189</sup> <sub>-174</sub>	0.20 <sup>+0.05</sup> <sub>-0.04</sub>	2.35 <sup>+0.08</sup> <sub>-0.08</sub>	0.17 <sup>+0.02</sup> <sub>-0.02</sub>	0.45 <sup>+0.03</sup> <sub>-0.03</sub>
A1644	4.70 <sup>+0.90</sup> <sub>-0.70</sub>	0.04	0.579 <sup>+0.111</sup> <sub>-0.074</sub>	211.3 <sup>+90.6</sup> <sub>-65.9</sub>	1, 830 <sup>+937</sup> <sub>-958</sub>	0.82 <sup>+0.62</sup> <sub>-0.62</sub>	5.39 <sup>+1.79</sup> <sub>-1.26</sub>	0.59 <sup>+0.28</sup> <sub>-0.23</sub>	0.98 <sup>+0.64</sup> <sub>-0.45</sub>
A1650	6.70 <sup>+0.80</sup> <sub>-0.80</sub>	0.08	0.704 <sup>+0.131</sup> <sub>-0.081</sub>	197.9 <sup>+73.7</sup> <sub>-51.2</sub>	1, 600 <sup>+714</sup> <sub>-758</sub>	0.69 <sup>+0.52</sup> <sub>-0.47</sub>	8.16 <sup>+2.36</sup> <sub>-1.65</sub>	0.85 <sup>+0.38</sup> <sub>-0.31</sub>	2.81 <sup>+1.53</sup> <sub>-1.07</sub>
A1651	6.10 <sup>+0.40</sup> <sub>-0.40</sub>	0.15	0.643 <sup>+0.014</sup> <sub>-0.013</sub>	127.5 <sup>+8.9</sup> <sub>-10.1</sub>	1, 725 <sup>+151</sup> <sub>-168</sub>	0.81 <sup>+0.12</sup> <sub>-0.13</sub>	7.38 <sup>+0.53</sup> <sub>-0.53</sub>	0.81 <sup>+0.08</sup> <sub>-0.08</sub>	2.03 <sup>+0.28</sup> <sub>-0.28</sub>
COMA	8.38 <sup>+0.34</sup> <sub>-0.34</sub>	0.06	0.654 <sup>+0.019</sup> <sub>-0.021</sub>	242.3 <sup>+18.6</sup> <sub>-20.1</sub>	1, 954 <sup>+201</sup> <sub>-202</sub>	1.13 <sup>+0.18</sup> <sub>-0.19</sub>	11.57 <sup>+0.67</sup> <sub>-0.70</sub>	1.38 <sup>+0.13</sup> <sub>-0.13</sub>	3.81 <sup>+0.42</sup> <sub>-0.44</sub>
NGC5044	1.07 <sup>+0.01</sup> <sub>-0.01</sub>	0.67	0.524 <sup>+0.002</sup> <sub>-0.003</sub>	7.7 <sup>+0.8</sup> <sub>-0.8</sub>	487 <sup>+50</sup> <sub>-53</sub>	0.15 <sup>+0.02</sup> <sub>-0.03</sub>	0.300 <sup>+0.003</sup> <sub>-0.004</sub>	0.10 <sup>+0.01</sup> <sub>-0.01</sub>	0.043 <sup>+0.001</sup> <sub>-0.001</sub>
A1736	3.50 <sup>+0.40</sup> <sub>-0.40</sub>	0.03	0.542 <sup>+0.147</sup> <sub>-0.092</sub>	263.4 <sup>+125.8</sup> <sub>-92.7</sub>	1, 889 <sup>+1110</sup> <sub>-1229</sub>	0.82 <sup>+0.66</sup> <sub>-0.66</sub>	3.85 <sup>+1.54</sup> <sub>-1.03</sub>	0.42 <sup>+0.23</sup> <sub>-0.19</sub>	0.48 <sup>+0.38</sup> <sub>-0.25</sub>
A3558	5.50 <sup>+0.40</sup> <sub>-0.40</sub>	0.09	0.580 <sup>+0.006</sup> <sub>-0.005</sub>	157.7 <sup>+7.5</sup> <sub>-9.6</sub>	2, 021 <sup>+106</sup> <sub>-134</sub>	1.14 <sup>+0.10</sup> <sub>-0.12</sub>	7.03 <sup>+0.52</sup> <sub>-0.52</sub>	0.84 <sup>+0.07</sup> <sub>-0.07</sub>	1.37 <sup>+0.20</sup> <sub>-0.20</sub>
A3562	5.16 <sup>+0.16</sup> <sub>-0.16</sub>	0.11	0.472 <sup>+0.006</sup> <sub>-0.006</sub>	69.7 <sup>+4.6</sup> <sub>-5.3</sub>	1, 926 <sup>+151</sup> <sub>-167</sub>	0.83 <sup>+0.09</sup> <sub>-0.10</sub>	5.14 <sup>+0.18</sup> <sub>-0.18</sub>	0.56 <sup>+0.03</sup> <sub>-0.04</sub>	0.81 <sup>+0.06</sup> <sub>-0.06</sub>
A3571	6.90 <sup>+0.20</sup> <sub>-0.20</sub>	0.14	0.613 <sup>+0.010</sup> <sub>-0.010</sub>	127.5 <sup>+7.3</sup> <sub>-8.7</sub>	1, 897 <sup>+137</sup> <sub>-154</sub>	1.02 <sup>+0.12</sup> <sub>-0.14</sub>	8.76 <sup>+0.32</sup> <sub>-0.32</sub>	1.02 <sup>+0.06</sup> <sub>-0.07</sub>	2.37 <sup>+0.17</sup> <sub>-0.17</sub>
A1795	7.80 <sup>+1.00</sup> <sub>-1.00</sub>	0.5	0.596 <sup>+0.003</sup> <sub>-0.002</sub>	54.9 <sup>+2.4</sup> <sub>-3.2</sub>	1, 773 <sup>+81</sup> <sub>-107</sub>	0.83 <sup>+0.07</sup> <sub>-0.09</sub>	9.03 <sup>+0.16</sup> <sub>-0.16</sub>	0.99 <sup>+0.13</sup> <sub>-0.14</sub>	2.84 <sup>+0.69</sup> <sub>-0.69</sub>
A3581	1.83 <sup>+0.04</sup> <sub>-0.04</sub>	0.31	0.543 <sup>+0.024</sup> <sub>-0.022</sub>	24.6 <sup>+3.7</sup> <sub>-3.1</sub>	840 <sup>+174</sup> <sub>-169</sub>	0.08 <sup>+0.02</sup> <sub>-0.02</sub>	0.92 <sup>+0.06</sup> <sub>-0.06</sub>	0.05 <sup>+0.01</sup> <sub>-0.01</sub>	0.14 <sup>+0.02</sup> <sub>-0.02</sub>
MKW8	3.29 <sup>+0.23</sup> <sub>-0.23</sub>	0.05	0.511 <sup>+0.098</sup> <sub>-0.059</sub>	75.4 <sup>+49.4</sup> <sub>-29.9</sub>	977 <sup>+703</sup> <sub>-619</sub>	0.11 <sup>+0.12</sup> <sub>-0.12</sub>	1.79 <sup>+0.50</sup> <sub>-0.32</sub>	0.11 <sup>+0.06</sup> <sub>-0.05</sub>	0.38 <sup>+0.21</sup> <sub>-0.13</sub>
A2029	9.10 <sup>+1.00</sup> <sub>-1.00</sub>	0.56	0.582 <sup>+0.004</sup> <sub>-0.004</sub>	58.5 <sup>+2.8</sup> <sub>-3.0</sub>	2, 200 <sup>+120</sup> <sub>-146</sub>	1.55 <sup>+0.14</sup> <sub>-0.17</sub>	12.77 <sup>+1.41</sup> <sub>-1.41</sub>	1.66 <sup>+0.19</sup> <sub>-0.20</sub>	3.71 <sup>+0.78</sup> <sub>-0.78</sub>
A2052	3.03 <sup>+0.04</sup> <sub>-0.04</sub>	0.52	0.526 <sup>+0.005</sup> <sub>-0.005</sub>	26.1 <sup>+1.8</sup> <sub>-2.0</sub>	1, 373 <sup>+107</sup> <sub>-119</sub>	0.34 <sup>+0.04</sup> <sub>-0.04</sub>	2.40 <sup>+0.05</sup> <sub>-0.05</sub>	0.21 <sup>+0.01</sup> <sub>-0.01</sub>	0.35 <sup>+0.01</sup> <sub>-0.01</sub>
MKW3S	3.70 <sup>+0.20</sup> <sub>-0.20</sub>	0.31	0.581 <sup>+0.008</sup> <sub>-0.007</sub>	46.5 <sup>+2.9</sup> <sub>-3.4</sub>	1, 257 <sup>+93</sup> <sub>-108</sub>	0.29 <sup>+0.03</sup> <sub>-0.04</sub>	2.96 <sup>+0.17</sup> <sub>-0.17</sub>	0.24 <sup>+0.02</sup> <sub>-0.02</sub>	0.62 <sup>+0.07</sup> <sub>-0.07</sub>
A2065	5.50 <sup>+0.40</sup> <sub>-0.40</sub>	0.04	1.162 <sup>+0.734</sup> <sub>-0.282</sub>	485.9 <sup>+254.4</sup> <sub>-133.8</sub>	1, 302 <sup>+780</sup> <sub>-1048</sub>	0.49 <sup>+0.49</sup> <sub>-0.49</sub>	8.01 <sup>+7.20</sup> <sub>-2.99</sub>	0.76 <sup>+0.76</sup> <sub>-0.76</sub>	3.83 <sup>+6.10</sup> <sub>-2.53</sub>
A2063	3.68 <sup>+0.11</sup> <sub>-0.11</sub>	0.12	0.561 <sup>+0.011</sup> <sub>-0.011</sub>	77.5 <sup>+5.9</sup> <sub>-6.1</sub>	1, 343 <sup>+127</sup> <sub>-130</sub>	0.33 <sup>+0.05</sup> <sub>-0.05</sub>	3.03 <sup>+0.12</sup> <sub>-0.12</sub>	0.26 <sup>+0.02</sup> <sub>-0.02</sub>	0.58 <sup>+0.05</sup> <sub>-0.05</sub>
A2142	9.70 <sup>+1.50</sup> <sub>-1.10</sub>	0.27	0.591 <sup>+0.006</sup> <sub>-0.006</sub>	108.5 <sup>+2.2</sup> <sub>-2.4</sub>	2, 537 <sup>+167</sup> <sub>-192</sub>	2.39 <sup>+0.26</sup> <sub>-0.30</sub>	15.93 <sup>+2.47</sup> <sub>-1.82</sub>	2.32 <sup>+0.38</sup> <sub>-0.29</sub>	4.36 <sup>+1.30</sup> <sub>-0.96</sub>
15	4.91 <sup>+0.28</sup> <sub>-0.28</sub>	0.03	0.444 <sup>+0.071</sup> <sub>-0.046</sub>	167.6 <sup>+72.9</sup> <sub>-46.7</sub>	2, 360 <sup>+125</sup> <sub>-1201</sub>	1.43 <sup>+0.91</sup> <sub>-0.82</sub>	5.62 <sup>+1.31</sup> <sub>-0.88</sub>	0.71 <sup>+0.26</sup> <sub>-0.21</sub>	0.65 <sup>+0.30</sup> <sub>-0.20</sub>
A2163	13.29 <sup>+0.64</sup> <sub>-0.64</sub>	0.1	0.796 <sup>+0.030</sup> <sub>-0.028</sub>						

**Table 1** – *continued* X-RAY CLUSTER PROPERTIES OF THE Complete Sample:

Cluster	$T$ [keV]	$\rho_0$ [ $10^{-25}$ g/cm $^3$ ]	$\beta$	$r_c$ [kpc]	$r_{out}$ [kpc]	$M_{gas}$ [ $10^{14} M_\odot$ ]	$M_N$ [ $10^{14} M_\odot$ ]	$M_{MSTG}$ [ $10^{14} M_\odot$ ]	$M_{MOND}$ [ $10^{14} M_\odot$ ]
(1)	(2)	(3)	(4)	(5)	(6)	(7)	(8)	(9)	(10)
S1101	3.00 $^{+1.20}_{-0.70}$	0.55	0.639 $^{+0.006}_{-0.007}$	39.4 $^{+2.2}_{-2.6}$	1,064 $^{+70}_{-78}$	0.20 $^{+0.02}_{-0.03}$	2.23 $^{+0.89}_{-0.52}$	0.17 $^{+0.07}_{-0.04}$	0.50 $^{+0.39}_{-0.33}$
A2589	3.70 $^{+0.20}_{-1.10}$	0.12	0.596 $^{+0.013}_{-0.012}$	83.1 $^{+6.6}_{-6.8}$	1,206 $^{+116}_{-121}$	0.25 $^{+0.04}_{-0.04}$	2.90 $^{+1.33}_{-0.87}$	0.23 $^{+0.14}_{-0.07}$	0.65 $^{+0.76}_{-0.38}$
A2597	4.40 $^{+0.40}_{-0.70}$	0.71	0.633 $^{+0.008}_{-0.008}$	40.8 $^{+2.2}_{-2.7}$	1,296 $^{+91}_{-103}$	0.36 $^{+0.04}_{-0.05}$	3.96 $^{+0.37}_{-0.63}$	0.34 $^{+0.04}_{-0.06}$	1.04 $^{+0.19}_{-0.32}$
A2634	3.70 $^{+0.28}_{-0.28}$	0.02	0.640 $^{+0.051}_{-0.043}$	256.3 $^{+32.8}_{-31.0}$	1,225 $^{+208}_{-219}$	0.25 $^{+0.06}_{-0.06}$	3.05 $^{+0.41}_{-0.37}$	0.24 $^{+0.04}_{-0.04}$	0.69 $^{+0.18}_{-0.17}$
A2657	3.70 $^{+0.30}_{-0.30}$	0.1	0.556 $^{+0.008}_{-0.007}$	83.8 $^{+5.0}_{-5.9}$	1,307 $^{+90}_{-105}$	0.30 $^{+0.03}_{-0.04}$	2.94 $^{+0.25}_{-0.24}$	0.24 $^{+0.02}_{-0.02}$	0.57 $^{+0.09}_{-0.09}$
A4038	3.15 $^{+0.03}_{-0.03}$	0.26	0.541 $^{+0.009}_{-0.008}$	41.5 $^{+3.3}_{-3.7}$	1,274 $^{+121}_{-134}$	0.28 $^{+0.04}_{-0.04}$	2.38 $^{+0.06}_{-0.05}$	0.19 $^{+0.01}_{-0.01}$	0.40 $^{+0.02}_{-0.02}$
A4059	4.40 $^{+0.30}_{-0.30}$	0.2	0.582 $^{+0.010}_{-0.010}$	63.4 $^{+4.4}_{-5.0}$	1,324 $^{+116}_{-126}$	0.33 $^{+0.05}_{-0.05}$	3.71 $^{+0.27}_{-0.27}$	0.32 $^{+0.03}_{-0.03}$	0.88 $^{+0.12}_{-0.12}$
A2734	3.85 $^{+0.62}_{-0.54}$	0.06	0.624 $^{+0.034}_{-0.029}$	149.3 $^{+19.4}_{-18.3}$	1,357 $^{+226}_{-234}$	0.36 $^{+0.09}_{-0.09}$	3.53 $^{+0.63}_{-0.55}$	0.31 $^{+0.07}_{-0.06}$	0.76 $^{+0.27}_{-0.23}$
A2877	3.50 $^{+2.20}_{-1.10}$	0.03	0.566 $^{+0.029}_{-0.025}$	133.8 $^{+14.5}_{-14.1}$	943 $^{+132}_{-139}$	0.11 $^{+0.02}_{-0.02}$	2.01 $^{+1.27}_{-0.64}$	0.13 $^{+0.08}_{-0.04}$	0.51 $^{+0.62}_{-0.31}$
NGC499	0.72 $^{+0.03}_{-0.02}$	0.2	0.722 $^{+0.034}_{-0.030}$	16.9 $^{+1.6}_{-1.7}$	196 $^{+27}_{-30}$	.001 $^{+0.000}_{-0.000}$	.111 $^{+0.009}_{-0.007}$	.002 $^{+0.000}_{-0.000}$	.035 $^{+0.005}_{-0.004}$
AWM7	3.75 $^{+0.09}_{-0.09}$	0.09	0.671 $^{+0.027}_{-0.025}$	121.8 $^{+13.7}_{-12.6}$	1,120 $^{+157}_{-154}$	0.22 $^{+0.05}_{-0.05}$	3.05 $^{+0.19}_{-0.18}$	0.23 $^{+0.03}_{-0.03}$	0.83 $^{+0.10}_{-0.09}$
PERSEUS	6.79 $^{+0.12}_{-0.12}$	0.63	0.540 $^{+0.006}_{-0.004}$	45.1 $^{+2.4}_{-2.9}$	2,414 $^{+145}_{-189}$	1.88 $^{+0.18}_{-0.22}$	9.70 $^{+0.23}_{-0.20}$	1.33 $^{+0.06}_{-0.07}$	1.83 $^{+0.08}_{-0.07}$
S405	4.21 $^{+0.67}_{-0.59}$	0.02	0.664 $^{+0.263}_{-0.133}$	323.2 $^{+185.0}_{-113.4}$	1,561 $^{+189}_{-165}$	0.53 $^{+0.53}_{-0.46}$	4.59 $^{+2.68}_{-1.47}$	0.44 $^{+0.33}_{-0.33}$	0.97 $^{+1.11}_{-0.12}$
3C129	5.60 $^{+0.70}_{-0.60}$	0.03	0.601 $^{+0.260}_{-0.131}$	223.9 $^{+123.7}_{-76.4}$	1,567 $^{+1133}_{-1455}$	0.52 $^{+0.52}_{-0.52}$	5.67 $^{+3.54}_{-1.85}$	0.55 $^{+0.43}_{-0.34}$	1.46 $^{+1.76}_{-0.92}$
A0539	3.24 $^{+0.09}_{-0.38}$	0.06	0.561 $^{+0.020}_{-0.018}$	104.2 $^{+10.2}_{-10.3}$	1,194 $^{+150}_{-158}$	0.23 $^{+0.04}_{-0.04}$	2.36 $^{+0.14}_{-0.13}$	0.18 $^{+0.02}_{-0.02}$	0.44 $^{+0.05}_{-0.05}$
S540	2.40 $^{+0.38}_{-0.34}$	0.08	0.641 $^{+0.073}_{-0.051}$	91.5 $^{+27.0}_{-21.1}$	877 $^{+305}_{-305}$	0.10 $^{+0.06}_{-0.05}$	1.46 $^{+0.33}_{-0.27}$	0.09 $^{+0.03}_{-0.03}$	0.31 $^{+0.14}_{-0.11}$
A0548w	1.20 $^{+0.19}_{-0.17}$	0.02	0.666 $^{+0.194}_{-0.111}$	139.4 $^{+63.7}_{-44.4}$	593 $^{+311}_{-328}$	.028 $^{+0.218}_{-0.18}$	.492 $^{+0.218}_{-0.137}$	.021 $^{+0.012}_{-0.009}$	.078 $^{+0.069}_{-0.043}$
A0548	3.10 $^{+0.10}_{-0.10}$	0.05	0.480 $^{+0.013}_{-0.013}$	83.1 $^{+9.2}_{-9.1}$	1,324 $^{+177}_{-175}$	0.27 $^{+0.05}_{-0.05}$	2.15 $^{+0.11}_{-0.11}$	0.17 $^{+0.02}_{-0.02}$	0.30 $^{+0.03}_{-0.03}$
A3395	5.00 $^{+0.30}_{-0.30}$	0.02	0.981 $^{+0.619}_{-0.244}$	473.2 $^{+270.5}_{-145.4}$	1,221 $^{+783}_{-977}$	0.30 $^{+0.30}_{-0.30}$	5.71 $^{+5.13}_{-2.21}$	0.48 $^{+0.48}_{-0.48}$	2.31 $^{+3.80}_{-1.64}$
UGC03957	2.58 $^{+0.41}_{-0.36}$	0.09	0.740 $^{+0.153}_{-0.086}$	100.0 $^{+23.9}_{-2.5}$	764 $^{+306}_{-339}$	0.08 $^{+0.05}_{-0.05}$	1.57 $^{+0.47}_{-0.34}$	0.09 $^{+0.04}_{-0.03}$	0.47 $^{+0.27}_{-0.19}$
PKS0745	7.21 $^{+0.11}_{-0.11}$	0.97	0.608 $^{+0.006}_{-0.006}$	50.0 $^{+2.5}_{-3.1}$	2,169 $^{+137}_{-159}$	1.59 $^{+0.17}_{-0.20}$	10.43 $^{+0.22}_{-0.22}$	1.36 $^{+0.07}_{-0.08}$	2.58 $^{+0.10}_{-0.10}$
A0644	7.90 $^{+0.80}_{-0.80}$	0.15	0.700 $^{+0.011}_{-0.011}$	143.0 $^{+7.8}_{-9.4}$	1,557 $^{+103}_{-119}$	0.66 $^{+0.08}_{-0.09}$	9.37 $^{+0.97}_{-0.97}$	0.97 $^{+0.11}_{-0.12}$	3.81 $^{+0.72}_{-0.72}$
S636	1.18 $^{+0.19}_{-0.17}$	0.01	0.752 $^{+0.217}_{-0.123}$	242.3 $^{+92.1}_{-62.1}$	742 $^{+323}_{-336}$	0.06 $^{+0.04}_{-0.02}$	0.65 $^{+0.29}_{-0.18}$	0.03 $^{+0.02}_{-0.01}$	0.09 $^{+0.08}_{-0.05}$
A1413	7.32 $^{+0.26}_{-0.24}$	0.19	0.660 $^{+0.017}_{-0.015}$	126.1 $^{+10.0}_{-10.5}$	1,794 $^{+179}_{-194}$	0.95 $^{+0.16}_{-0.17}$	9.46 $^{+0.48}_{-0.43}$	1.08 $^{+0.10}_{-0.10}$	3.03 $^{+0.29}_{-0.26}$
M49	0.95 $^{+0.02}_{-0.01}$	0.26	0.592 $^{+0.007}_{-0.007}$	7.7 $^{+0.8}_{-0.8}$	177 $^{+19}_{-20}$	.001 $^{+0.000}_{-0.000}$	.109 $^{+0.003}_{-0.002}$	.002 $^{+0.000}_{-0.000}$	.041 $^{+0.002}_{-0.001}$
A3528n	3.40 $^{+1.66}_{-0.64}$	0.07	0.621 $^{+0.034}_{-0.030}$	125.4 $^{+13.1}_{-13.3}$	1,181 $^{+129}_{-193}$	0.24 $^{+0.05}_{-0.06}$	2.71 $^{+0.34}_{-0.54}$	0.21 $^{+0.11}_{-0.05}$	0.59 $^{+0.57}_{-0.23}$
A3528s	3.15 $^{+0.89}_{-0.59}$	0.09	0.463 $^{+0.013}_{-0.012}$	71.1 $^{+7.0}_{-6.9}$	1,872 $^{+244}_{-250}$	0.75 $^{+0.12}_{-0.13}$	2.99 $^{+0.85}_{-0.57}$	0.32 $^{+0.09}_{-0.07}$	0.29 $^{+0.17}_{-0.11}$
A3530	3.89 $^{+0.27}_{-0.25}$	0.03	0.773 $^{+0.114}_{-0.085}$	296.5 $^{+54.3}_{-46.1}$	1,150 $^{+282}_{-308}$	0.23 $^{+0.08}_{-0.07}$	3.56 $^{+0.79}_{-0.60}$	0.28 $^{+0.07}_{-0.06}$	1.05 $^{+0.44}_{-0.34}$
A3532	4.58 $^{+0.19}_{-0.17}$	0.05	0.653 $^{+0.034}_{-0.029}$	198.6 $^{+20.8}_{-20.3}$	1,372 $^{+188}_{-199}$	0.38 $^{+0.08}_{-0.08}$	4.41 $^{+0.37}_{-0.32}$	0.39 $^{+0.05}_{-0.05}$	1.15 $^{+0.19}_{-0.16}$
A1689	9.23 $^{+0.28}_{-0.28}$	0.33	0.690 $^{+0.021}_{-0.011}$	114.8 $^{+6.9}_{-7.7}$	1,898 $^{+143}_{-154}$	1.23 $^{+0.17}_{-0.18}$	13.21 $^{+0.50}_{-0.50}$	1.61 $^{+0.11}_{-0.12}$	5.14 $^{+0.36}_{-0.36}$
A3560	3.16 $^{+0.51}_{-0.44}$	0.03	0.566 $^{+0.033}_{-0.029}$	180.3 $^{+22.5}_{-21.6}$	1,402 $^{+230}_{-240}$	0.35 $^{+0.08}_{-0.08}$	2.71 $^{+0.49}_{-0.42}$	0.23 $^{+0.04}_{-0.04}$	0.42 $^{+0.15}_{-0.15}$
A1775	3.69 $^{+0.20}_{-0.11}$	0.06	0.673 $^{+0.026}_{-0.023}$	183.1 $^{+15.3}_{-16.3}$	1,391 $^{+153}_{-167}$	0.42 $^{+0.07}_{-0.08}$	3.72 $^{+0.29}_{-0.21}$	0.34 $^{+0.04}_{-0.03}$	0.81 $^{+0.12}_{-0.09}$
A1800	4.02 $^{+0.64}_{-0.56}$	0.04	0.766 $^{+0.308}_{-0.139}$	276.1 $^{+157.5}_{-94.2}$	1,284 $^{+825}_{-949}$	0.34 $^{+0.36}_{-0.23}$	4.14 $^{+2.45}_{-1.23}$	0.36 $^{+0.27}_{-0.15}$	1.15 $^{+1.31}_{-0.66}$
A1914	10.53 $^{+0.51}_{-0.50}$	0.22	0.751 $^{+0.018}_{-0.017}$	162.7 $^{+10.4}_{-11.6}$	1,768 $^{+148}_{-162}$	1.08 $^{+0.16}_{-0.18}$	15.21 $^{+0.90}_{-0.87}$	1.79 $^{+0.16}_{-0.16}$	7.44 $^{+0.77}_{-0.75}$
NGC5813	0.52 $^{+0.08}_{-0.07}$	0.18	0.766 $^{+0.179}_{-0.103}$	17.6 $^{+6.4}_{-4.3}$	166 $^{+79}_{-97}$	.001 $^{+0.001}_{-0.001}$	.072 $^{+0.026}_{-0.017}$	.001 $^{+0.001}_{-0.000}$	.021 $^{+0.014}_{-0.009}$
NGC5846	0.82 $^{+0.01}_{-0.01}$	0.47	0.599 $^{+0.016}_{-0.015}$	4.9 $^{+0.7}_{-0.8}$	152 $^{+26}_{-27}$	.001 $^{+0.000}_{-0.000}$	.082 $^{+0.003}_{-0.003}$	.001 $^{+0.000}_{-0.000}$	.031 $^{+0.002}_{-0.002}$
A2151w	2.40 $^{+0.06}_{-0.06}$	0.16	0.564 $^{+0.014}_{-0.013}$	47.9 $^{+4.1}_{-4.4}$	957 $^{+105}_{-114}$	0.12 $^{+0.02}_{-0.02}$	1.42 $^{+0.06}_{-0.06}$	0.09 $^{+0.01}_{-0.01}$	0.25 $^{+0.02}_{-0.02}$
A3627	6.02 $^{+0.08}_{-0.08}$	0.04	0.555 $^{+0.056}_{-0.044}$	210.6 $^{+40.4}_{-36.5}$	1,830 $^{+474}_{-515}$	0.78 $^{+0.28}_{-0.29}$	6.62 $^{+0.95}_{-0.75}$	0.71 $^{+0.15}_{-0.14}$	1.47 $^{+0.41}_{-0.32}$
TRIANGUL	9.60 $^{+0.60}_{-0.60}$	0.1	0.610 $^{+0.010}_{-0.010}$	196.5 $^{+11.4}_{-13.1}$	2,385 $^{+169}_{-187}$	1.98 $^{+0.22}_{-0.25}$	15.22 $^{+1.01}_{-1.01}$	2.11 $^{+0.17}_{-0.18}$	4.48 $^{+0.57}_{-0.57}$
OPHIUCHU	10.26 $^{+0.32}_{-0.32}$	0.13	0.747 $^{+0.035}_{-0.032}$	196.5 $^{+18.2}_{-19.0}$	1,701 $^{+224}_{-240}$	0.91 $^{+0.20}_{-0.21}$	14.11 $^{+1.03}_{-0.96}$	1.59 $^{+0.19}_{-0.19}$	6.91 $^{+0.89}_{-0.83}$
ZwC174	5.23 $^{+0.84}_{-0.73}$	0.1	0.717 $^{+0.073}_{-0.053}$	163.4 $^{+33.1}_{-28.3}$	1,354 $^{+349}_{-378}$	0.43 $^{+0.19}_{-0.18}$	5.49 $^{+1.18}_{-0.96}$	0.50 $^{+0.15}_{-0.13}$	1.79 $^{+0.73}_{-0.59}$
A2319	8.80 $^{+0.50}_{-0.50}$	0.1	0.591 $^{+0.013}_{-0.012}$	200.7 $^{+13.5}_{-15.0}$	2,657 $^{+228}_{-250}$	2.66 $^{+0.35}_{-0.39}$	15.07 $^{+0.98}_{-0.98}$	2.25 $^{+0.19}_{-0.20}$	3.60 $^{+0.45}_{-0.45}$
A3695	5.29 $^{+0.85}_{-0.74}$	0.04	0.642 $^{+0.259}_{-0.177}$	281.0 $^{+179.3}_{-106.1}$	1,887 $^{+1379}_{-1379}$	0.96 $^{+0.96}_{-0.96}$	6.88 $^{+4.08}_{-2.34}$	0.79 $^{+0.62}_{-0.46}$	1.49 $^{+1.73}_{-0.86}$
IIZw108	3.44 $^{+0.55}_{-0.48}$	0.03	0.662 $^{+0.167}_{-0.097}$	257.0 $^{+112.5}_{-75.3}$	1,327 $^{+690}_{-675}$	0.33 $^{+0.26}_{-0.22}$	3.19 $^{+2.25}_{-0.80}$	0.27 $^{+0.11}_{-0.11}$	0.65 $^{+0.50}_{-0.32}$
A3822	4.90 $^{+0.78}_{-0.69}$	0.04	0.639 $^{+0.150}_{-0.093}$	247.2 $^{+113.2}_{-79.4}$	1,675 $^{+904}_{-942}$	0.67 $^{+0.57}_{-0.52}$	5.63 $^{+2.07}_{-1.41}$	0.58 $^{+0.31}_{-0.25}$	1.27 $^{+0.91}_{-0.62}$
A3827	7.08 $^{+1.13}_{-0.99}$	0.05	0.989 $^{+0.410}_{-0.192}$	417.6 $^{+175.5}_{-107.5}$	1,515 $^{+762}_{-977}$	0.74 $^{+0.74}_{-0.74}$	10.81 $^{+6.58}_{-3.39}$	1.15 $^{+1.15}_{-1.15}$	5.16 $^{+5.57}_{-2.87}$
A3888	8.84 $^{+1.41}_{-1.24}$	0.1	0.928 $^{+0.084}_{-0.066}$	282.4 $^{+34.5}_{-32.4}$	1,455 $^{+252}_{-281}$	0.71 $^{+0.71}_{-0.71}$	12.61 $^{+2.58}_{-2.18}$	1.33 $^{+1.33}_{-1.33}$	7.14 $^{+2.45}_{-2.07}$
A3921	5.73 $^{+0.24}_{-0.23}$	0.07	0.762 $^{+0.036}_{-0.030}$	231.0 $^{+20.7}_{-20.8}$	1,435 $^{+167}_{-182}$	0.52 $^{+0.10}_{-0.10}$	6.70 $^{+0.53}_{-0.46}$	0.65 $^{+0.07}_{-0.07}$	2.35 $^{+0.35}_{-0.30}$
HCG94	3.45 $^{+0.30}_{-0.30}$	0.11	0.514 $^{+0.007}_{-0.006}$	60.6 $^{+3.8}_{-4.4}$	1,237 $^{+89}_{-114}$	0.24 $^{+0.03}_{-0.03}$	2.40 $^{+0.21}_{-0.21}$	0.19 $^{+0.02}_{-0.02}$	0.43 $^{+0.07}_{-0.07}$
RXJ2344	4.73 $^{+0.76}_{-0.66}$	0.07	0.807 $^{+0.033}_{-0.030}$	212.0 $^{+16.7}_{-17.4}$	1,222 $^{+127}_{-135}$	0.34 $^{+0.05}_{-0.06}$	4.97 $^{+0.85}_{-0.74}$	0.43 $^{+0.08}_{-0.07}$	1.78 $^{+0.57}_{-0.50}$

Note — We have adopted the compilation of Reiprich (2001); Reiprich & Böhringer (2002) as our sample.

Column (1)	Galaxy cluster name (truncated to 8 characters)	Column (6)	radius where $\rho_{gas} \approx 10^{-28}$ g/cm $^3$
Column (2)	X-ray temperature	Column (7)	ICM gas mass integrated to $r_{out}$
Column (3)			